Organic Geochemistry 195 (2024) 104812

Contents lists available at ScienceDirect

Organic Geochemistry

journal homepage: www.elsevier.com/locate/orggeochem

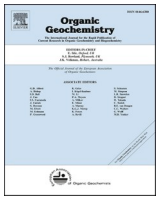

Assessment of branched glycerol monoalkyl glycerol tetraether (brGMGT)-based paleothermometry in the 250,000-year sediment record of Lake Chala, equatorial East Africa

A.J. Baxter [a], F. Peterse [a,*], D. Verschuren [b], J.S. Sinninghe Damsté [a,c]

[a] Utrecht University, Department of Earth Sciences, Princetonlaan 8A, Utrecht 3584 CB, the Netherlands
[b] Ghent University, Department of Biology, Limnology Unit, K.L. Ledeganckstraat 35, Gent B-9000, Belgium
[c] NIOZ Royal Netherlands Institute for Sea Research, Department of Marine Microbiology and Biogeochemistry, PO Box 59, Den Burg 1790 AB, the Netherlands

ARTICLE INFO

Associate Editor: Isla Castañeda

Keywords:
brGMGTs
H-shaped GDGTs
brGDGTs
Lake sediments
Paleoclimate
East Africa
Lake Chala
ICDP
DeepCHALLA

ABSTRACT

Branched glycerol monoalkyl glycerol tetraethers (brGMGTs), a relatively understudied group of bacterial membrane lipids structurally similar to branched glycerol dialkyl glycerol tetraethers (brGDGTs), appear to be strongly influenced by temperature in terrestrial settings. In surficial bottom sediments of East African lakes, the abundance of brGMGTs relative to the sum of brGMGTs and brGDGTs (%brGMGT) and brGMGT distribution are strongly related to local mean annual air temperature (MAAT), stimulating development of new paleothermometers. However, applications of these methods to lake-sediment records are currently lacking. Here we investigate brGMGT concentrations and distributions in 916 samples throughout the 250,000-year (250-kyr) sediment sequence from Lake Chala, a presently fresh and permanently stratified (meromictic) tropical crater lake. All seven previously identified brGMGTs occur abundantly, reflected in a relatively high average %brGMGT of 19%. BrGMGTs and brGDGTs concentrations throughout the sequence are strongly correlated ($R = 0.83$, $p < 0.001$), suggesting that their producers and/or associated ecological niches substantially overlap. Clear distinction can be made between brGMGTs produced predominantly in the bottom sediments (H1034a and H1034c) versus the anoxic lower water column (H1020a-c and H1034b). Although a 17-month monitoring study of Lake Chala suggested brGMGTs are primarily produced in the sediments, down-core data assign greater importance to aquatic production than previously estimated. Instead of reflecting temperature, %brGMGT variations showed greatest similarity to GDGT proxies reflecting lake depth and/or mixing regime. BrGMGT-based temperature models produce ambiguous reconstructions, showing little similarity to known global temperature trends or the brGDGT-based mean summer temperature (MST) reconstruction from the same sediments.

1. Introduction

In order to fully understand Earth's dynamic climate system, and to decrease uncertainty in projections of future climate change, it is essential to have accurate estimates of past temperature variability from around the globe. To date, the majority of techniques for quantifying past temperatures, and the bulk of resulting reconstructions, characterize temperature variability in marine or polar settings. However, as temperature history on individual continents can differ considerably from this 'global' view (Otto-Bliesner et al., 2006; Blome et al., 2012; Loomis et al., 2017), it is important to obtain trustworthy records from the many underrepresented continental settings. Lipid biomarkers form the basis of several paleothermometers applicable to the terrestrial realm and have become essential tools for estimating past temperature variability (Castañeda and Schouten, 2011; Inglis et al., 2022). For example, the unsaturation index of C_{37} alkenones (U^{K}_{37}), a ratio between di- and tri-unsaturated ketones produced by haptophyte algae, was found to be strongly related to sea surface temperature (SST) in marine settings (Brassell et al., 1986; Prahl and Wakeham, 1987) with later studies demonstrating that this paleothermometer functions similarly in lakes (Zink et al., 2001). Likewise, the TetraEther index of 86 carbon atoms (TEX_{86}) paleothermometer was originally based on empirical relations from marine sediments which showed that the synthesis of cyclopentane rings in isoprenoid glycerol dialkyl glycerol tetraethers (isoGDGTs) of aquatic Thaumarchaeota is temperature dependent, and

* Corresponding author.
E-mail address: f.peterse@uu.nl (F. Peterse).

https://doi.org/10.1016/j.orggeochem.2024.104812
Received 11 January 2024; Received in revised form 24 May 2024; Accepted 27 May 2024
Available online 31 May 2024

can be used to reconstruct past sea (sub) surface temperature (Schouten et al., 2002; Huguet et al., 2007; Kim et al., 2010). Subsequent research on lakes suggested that past changes in lake surface temperature (LST) could also be estimated from the TEX_{86} signal in lacustrine sediments (Powers et al., 2004; Powers et al., 2010). Moreover, the distribution of branched (br) GDGTs, membrane lipids of bacteria (Chen et al., 2022; Halamka et al., 2023) that thrive in soils (Weijers et al., 2006), peats (Sinninghe Damsté et al., 2000; Weijers et al., 2006; Naafs et al., 2017), and lakes (Blaga et al., 2009; Tierney et al., 2010; Pearson et al., 2011) is temperature-sensitive. BrGDGTs have been applied as organic paleothermometers, where their degree of methylation in surface sediments from virtually all continental settings is strongly correlated to temperature (Weijers et al., 2007; De Jonge et al., 2014; Raberg et al., 2022), albeit with a varying slope, hence requiring setting-specific calibrations.

In addition to the more established lipid paleothermometers described above, a lesser-known group of membrane spanning lipids, the glycerol monoalkyl glycerol tetraethers (GMGTs), also referred to as the H-shaped GDGTs, or H-GDGTs, have shown potential as temperature proxy (Naafs et al., 2018; Baxter et al., 2019). Their structure is similar to that of the regular GDGTs, but with an additional carbon bond connecting the two alkyl chains (Fig. 1), which is theorized to be an adaptation to heat stress because it increases membrane stability at higher temperatures (Morii et al., 1998). Their initial discovery relates to the identification of an isoprenoid (iso) GMGT without cyclopentane moieties (isoGMGT-0) in a hyperthermophilic methanogen (Morii et al., 1998). To date, forms with up to six cyclopentane moieties have been identified in extremophilic Crenarchaeota and Euryarchaeota cultivated from settings such as (hydro) thermal vents and hot springs (Schouten et al., 2008; Knappy et al., 2011). IsoGMGTs have been detected in (hydro) thermal (Jaeschke et al., 2012; Jia et al., 2014; Bauersachs and Schwark, 2016; Pan et al., 2016) as well as moderate to low-temperature environments, such as in lacustrine and marine sediments (Schouten et al., 2008; Liu et al., 2012; Pan et al., 2016), and also peats (Naafs et al., 2018), where their modern-day abundance relative to the regular isoGDGTs (%isoGMGT) was found to be positively correlated to local mean annual air temperature (MAAT).

Besides isoGMGTs, also brGMGTs have been reported in marine sediments (Liu et al., 2012; Xie et al., 2014; Sluijs et al., 2020; Bijl et al., 2021; Cramwinckel et al., 2022; Frieling et al., 2023), lakes (Baxter et al., 2019; Baxter et al., 2021), rivers (Kirkels et al., 2022), peats (Naafs et al., 2018; Tang et al., 2021; Elling et al., 2023), and soils (Baxter et al., 2021; Kirkels et al., 2022), although (limited) data from soils suggests that they are not ubiquitous in that context. Their exact structure has not yet been determined, but it is feasible that, like the brGDGTs (Sinninghe Damsté et al., 2000), brGMGTs consist of two C_{28} linear alkyl chains methylated at the C-13 and C-16 positions, where two mid-chain methyl groups of the opposing alkyl chains are joined by a covalent bond to form the bridge (Fig. 1), as is the case in isoGMGTs (Lutnaes et al., 2006). BrGMGTs supposedly containing two, three or four methyl groups have been identified, and are generally referred to as H1020, H1034 and H1048, respectively, in reference to their mass to charge ratios (m/z 1020, 1034, and 1048; Naafs et al., 2018; Baxter et al., 2019). The additional methyl groups in H1034 and H1048 presumably occur at either the C-5 or C-6 position, as is the case in penta- and hexamethylated forms of the brGDGTs (i.e., the 5- and 6-Me brGDGTs; De Jonge et al., 2013). The H1020 and H1034 brGMGTs display up to three isomers, labeled alphabetically based on their elution order (i.e., H1020a–c and H1034a–c; Baxter et al., 2019). In the case of H1034, the occurrence of isomers may relate to a different position of the additional methyl groups at either C-5 or C-6. However, in the case of H1020, the isomers probably reflect the two potential configurations of the bridge, formed between parallel or oppositely positioned mid-chain methyl groups across the alkyl chains (Fig. 1; Baxter et al., 2019). In combination with parallel and anti-parallel configurations of the two glycerol moieties of each GMGT, this could theoretically lead to four isomers. Unlike the brGDGTs which can possess 1–2 cyclopentane rings (Weijers et al., 2006), to date no cyclopentane moiety-containing brGMGTs have been detected in natural settings (Naafs et al., 2018; Baxter et al., 2019).

Members of the phylum Acidobacteria, a group of mainly heterotrophic bacteria common in soils and peat (Chen et al., 2022; Halamka et al., 2023; Sinninghe Damsté et al., 2011, 2014, 2018; Weijers et al., 2009), as well as other yet unidentified bacterial phyla (Weber et al., 2018; De Jonge et al., 2019; Sahonero-Canavesi et al., 2022) are the likely producers of brGDGTs in natural settings. On the other hand, relatively little is known about the producers of brGMGTs, as they have not yet been identified in bacterial cultures. Their apparent preference for anoxic niches in lakes and peats (Naafs et al., 2018; Baxter et al., 2021) and generally low abundance in aerated soils (Baxter et al., 2021; Kirkels et al., 2022) attests to production by anaerobic bacteria. Also the high abundance of brGMGTs relative to the sum of brGMGTs and brGDGTs (%brGMGT; Eq. 1) in the anoxic and water-saturated subsurface of peat deposits has been explained by anaerobic bacteria production (Naafs et al., 2018).

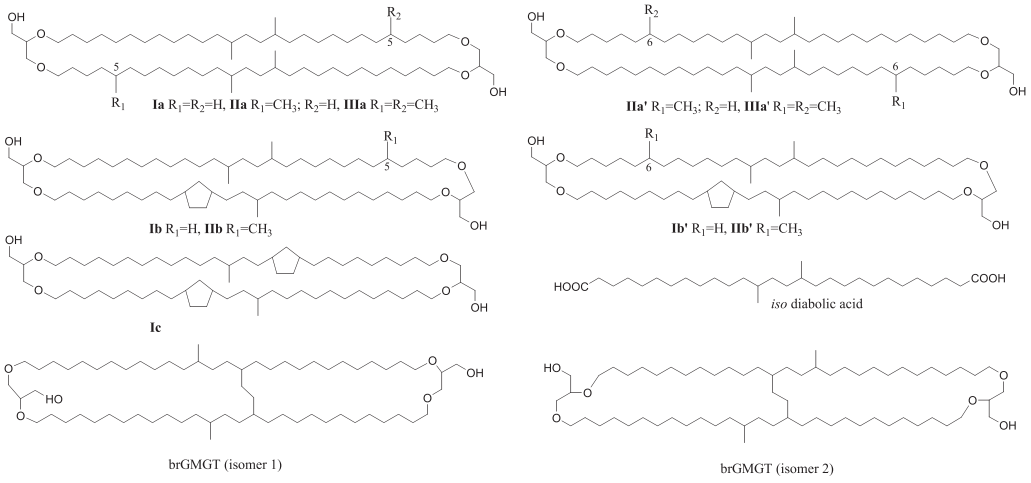

Fig. 1. Molecular structures of brGDGTs, *iso* diabolic acid (the precursor to brGDGTs), and the tentative structure of brGMGTs, assuming that, similarly to isoprenoid tetra acids (Lutnaes et al., 2006; Lutnaes et al., 2007), the bridge between the two alkyl chains is formed by a covalent bond between carbon atoms of two mid-chain methyl groups, as depicted previously in Baxter et al. (2021). The H1020 isomers theoretically resemble brGMGT isomer 1 or 2 as shown here, whereas H1034 and H1048 have one and two additional methyl groups, respectively. The precise positions of bridge and methyl groups are as yet undetermined. Presumably the methylation occurs at C-5 and C-6, as in brGDGTs.

$$\%brGMGT = \frac{\Sigma brGMGT}{(\Sigma brGMGT + \Sigma brGDGT)} * 100 \quad (1)$$

Recently, an archaeal enzyme responsible for bridge formation in isoGMGTs was identified (Garcia et al., 2023; Li et al., 2023) and found to be present in the genomes of strictly anaerobic archaea and metagenomes from oxygen-poor settings, but absent in oxic settings (Li et al., 2023). Homologs of this enzyme have also been found in the genomes of bacteria with the genetic potential to make brGDGTs (Garcia et al., 2023). Based on comparable $\delta^{13}C$ values of brGMGTs, brGDGTs and total organic carbon in peats and lignites, a heterotrophic source organism for both lipid groups was suggested (Elling et al., 2023). However, divergence between brGMGT and brGDGT $\delta^{13}C$ profiles across the oxic-anoxic gradient in peat sequences suggests that their sources do not fully overlap and/or that brGMGTs may have diverse sources (Elling et al., 2023).

Based on analysis of brGMGTs in recently deposited (surficial) bottom sediments from 70 lakes in East Africa (Baxter et al., 2019) and in 386 globally distributed peats (Naafs et al., 2018) the abundance of brGMGTs relative to brGDGTs in both settings appeared to relate to temperature, with higher %brGMGT values characterizing warmer environments. Despite the substantial scatter displayed by these relationships, especially in lakes and peats with MAAT > 20 °C, it was suggested that %brGMGT may be applied to lake sediment records as a semi-quantitative indicator of past temperature change (Baxter et al., 2019). Moreover, also the distribution of individual brGMGTs in the East African lake dataset appears to show temperature dependence (Baxter et al., 2019), prompting definition of the brGMGT Index (brGMGTI), which incorporates the positive (H1020c, H1034a and H1034c) or negative (H1020b and H1048) correlation between the fractional abundances of these respective brGMGTs and local MAAT (Baxter et al., 2019).

$$brGMGTI = \frac{([H1020c] + [H1034a] + [H1034c])}{([H1020b] + [H1020c] + [H1034a] + [H1034c] + [H1048])} \quad (2)$$

Linear regression of the brGMGTI to MAAT then created a first brGMGT-based temperature inference model for East African lakes (Baxter et al., 2019):

$$MAAT = 2.86 + 26.5 * brGMGTI \quad (3)$$

Additionally, a second temperature inference model was created based on a regression with stepwise forward selection (SFS) of individual brGMGTs (Baxter et al., 2019):

$$MAAT = 1.18 + 0.47 * [H1034a] + 0.12 * [H1020a] + 0.50 * [H1020c] \quad (4)$$

with values between the square brackets referring to the fractional abundances of the GMGTs. The more limited structural diversity of brGMGTs in peats, where no additional isomers of the three known brGMGTs have been documented (Naafs et al., 2018), does not allow application of these relationships in this setting.

An in-depth investigation into the occurrence and distribution of brGMGTs in the catchment soils, suspended particulate matter (SPM), settling particles and bottom sediments of Lake Chala, a permanently stratified (meromictic) crater lake in tropical East Africa, revealed that %brGMGT values were substantially higher in recently deposited profundal sediments than in the SPM and settling particles in the water column (Baxter et al., 2021). Moreover the brGMGT distributions were markedly different, suggesting that the sedimentary brGMGTs were not derived from those in the water column but are mainly produced in the lake sediments themselves. Hence, it was suggested that brGMGTs likely have a more restricted source than the brGDGTs extracted from the same sediments (Baxter et al., 2021), as the latter are also produced abundantly in the anoxic lower water column (van Bree et al., 2020) and in catchment soils (Sinninghe Damsté et al., 2008), erosion of which by high-intensity rainfall may represent an additional source for sedimentary brGDGTs in lakes. The restricted source of brGMGTs relative to brGDGTs was interpreted as potentially advantageous for bacterial-lipid based palaeothermometry in lakes (Baxter et al., 2021), warranting their further study. Indeed, several outstanding issues remain surrounding the effectiveness of brGMGTs as paleothermometer in lake-sediment records. Firstly, the large scatter observed in the relationship between % brGMGT and MAAT, particularly at MAAT > 20 °C, makes it uncertain if this proxy would accurately register past temperature variation through time in tropical lakes. Secondly, as currently available data suggest that brGMGTs are likely produced mostly in the sediments of lakes, the mechanism through which they record and track changes in air temperature over time must be resolved.

In 2016, International Continental Drilling Program (ICDP) project DeepCHALLA (Verschuren et al., 2013) recovered 214.8 m of laminated organic-rich, diatomaceous sediments from the bottom of Lake Chala, which constitute a continuous record of past lake dynamics and environmental change covering the last c. 250,000 years (250 kyr; Maitituerdi et al., 2022). In-depth modern-system studies of Lake Chala (Sinninghe Damsté et al., 2009; Buckles et al., 2014; van Bree et al., 2020; Baxter et al., 2021) revealed clear spatio-temporal niches of GDGT producers in the water column and facilitated assessment of existing paleothermometers as well as validation of the branched versus isoprenoid tetraether (BIT) index as a moisture balance proxy. At the same time, seismic reflection data, lithology and fossil diatom assemblages provided reconstructions of variation in lake depth, chemistry, mixing regime and water-column structure since the inception of this tropical crater lake. This combined knowledge enabled the influences of past climate change and lake-system evolution on GDGT variability throughout the DeepCHALLA record to be disentangled (Baxter et al., 2024). As additionally the brGMGT-inferred MAAT recorded in surficial bottom sediments of Lake Chala matches observed local mean annual air temperature within the uncertainty of the East African lake calibration (Baxter et al., 2021), the DeepCHALLA sediment record seemed ideal material for testing the robustness of brGMGT-based temperature proxies and determining the primary drivers of their fluctuations through time. Here we report on the concentrations and distribution of brGMGTs in 916 sediment horizons throughout the DeepCHALLA sequence, and on the results of diverse uni- and multivariate analyses aiming to assess their suitability for paleothermometry in lakes.

2. Study site: Lake Chala

2.1. Site description

Lake Chala (sometimes spelled 'Challa' after the nearby village) is a relatively small (4.2 km^2) and deep (90 m in 2016) volcanic crater lake in eastern equatorial Africa (3°19'S, 37°42'E), bridging the border between Kenya and Tanzania (Fig. 2). It is located ~880 m above sea level in the southeastern foothills of Mt. Kilimanjaro. The amount of average annual rainfall (565 mm yr^{-1}; De Wispelaere et al., 2017; Griepentrog et al., 2019) is greatly exceeded by evaporation from the lake surface (1735 mm yr^{-1}; Payne, 1970) and hence, the lake's water budget is additionally maintained by substantial subsurface inflow (Payne, 1970), which originates as rainfall on the forested and subalpine slopes of Mt. Kilimanjaro (Hemp, 2006; Bodé et al., 2020) and reaches the lake some 3–4 months later (Barker et al., 2011). Although the lake is topographically closed, a small creek breaching the north-western crater rim is sometimes activated during infrequent high rainfall events (Buckles et al., 2014). The steep crater walls reach up to 170 m above the lake's surface, and equally steep underwater slopes extend to ~60–70 m water depth before leveling off to form the flat central lake bottom (Moernaut et al., 2010). The lake's catchment area (5.6 km^2) is only marginally larger than its surface area.

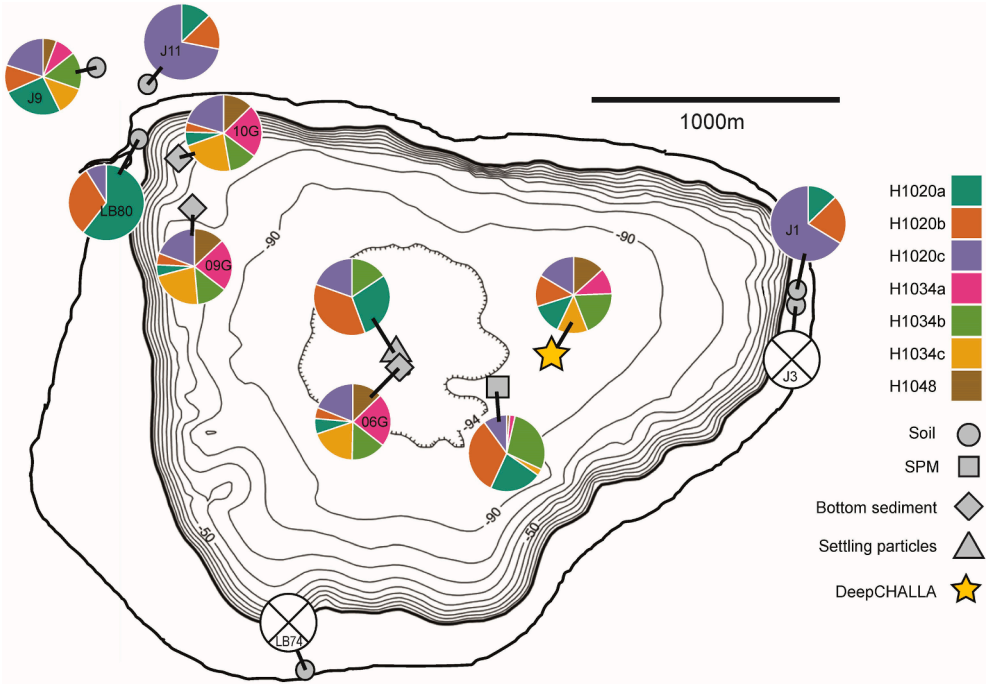

Fig. 2. Map of the Chala crater basin (outer thick black line) and lake bathymetry (depth contours; Moernaut et al., 2010) with the sampling locations (grey symbols) and brGMGT distributions (pie charts) of soils, bottom sediments, SPM and settling particles as reported by Baxter et al. (2021). In the case of SPM and settling particle series, the brGMGT fractional abundances are weighted to total brGMGTs concentration (μg g^{-1} C_{org}) and flux (ng m^{-2} day^{-1}), respectively. In soil samples marked with a black X, no brGMGTs were detected. The pie chart at the drill site of the DeepCHALLA sediment sequence (yellow star) shows the average fractional abundances of brGMGTs throughout the 250-kyr record.

The Lake Chala region has a semi-arid tropical climate regime. The highest mean monthly air temperatures are reached in February–March (night and daytime temperature of 21 and 33 °C), and the lowest in July–August (night and daytime temperature of 18 and 28 °C; Buckles et al., 2014). The area is characterized by a bimodal seasonal rainfall pattern (Wainwright et al., 2019 and references cited therein) related to the movement of the intertropical convergence zone (ITCZ) and associated tropical rain belt. The so-called 'short' and 'long rains' occur in late October–December and March–May, respectively, separated by the primary dry season in June–September (i.e., during austral winter) and the short dry season in January–February (i.e., during austral summer). This alternation between windy/dry and calm/wet seasons creates a strong seasonal pattern of mixing and stratification in Lake Chala. Modest wind speeds and high lake-surface temperatures stretching over both the short and long rain seasons (October–May) weaken mixing of the upper water column and promote stronger temperature stratification. During these months, oxygen renewal below the daily mixed layer is diminished and the oxycline shifts to a shallower position (~10 to 15 m), with most intensely stratified conditions occurring during austral summer (Wolff et al., 2014; van Bree et al., 2018; van Bree et al., 2020). Hence, as the size of the oxygen-rich surface layers shrinks, the relative proportion of the anoxic bottom water is increased. During the main dry season between the end of May and mid-September, greater wind speeds and lower air temperatures facilitate turbulent and convective deep mixing of the upper water column down to ~45–50 m depth, shifting the oxycline to a deep position (i.e., the relative size of the oxygenated portion is increased at the expense of the anoxic zone; Wolff et al., 2011; Buckles et al., 2014; van Bree et al., 2018; van Bree et al., 2020). This introduces nutrient-rich deep water to the nutrient-starved epilimnion, thus promoting phytoplankton productivity (for example triggering a pronounced diatom bloom; Wolff et al., 2014; van Bree et al., 2018). A period of shallower mixing to ~20–25 m depth during the short dry season (January–February) interrupts the long stratification period (Wolff et al., 2014; van Bree et al., 2018; van Bree et al., 2020). The lower water column of Lake Chala is chemically stratified and permanently anoxic below 60 m depth, promoting regular accumulation of organic diatomaceous sediments with distinct annual lamination (i.e., varves; Wolff et al., 2011).

2.2. The DeepCHALLA sediment sequence

The 214.8-m DeepCHALLA sediment sequence was extracted from the profundal lake bottom in overlapping 3-m sections, using hydraulic piston coring operated from a platform anchored in the deep eastern sector of the lake (Fig. 2). Construction of the master sediment sequence and sampling procedure for biomarkers has been described by (Baxter et al., 2024; Baxter et al., 2023). Formulation of an absolute-dated chronology for the full DeepCHALLA sequence is still underway. The present study uses a preliminary chronology based on high-resolution ^{14}C dating of the 25-kyr CHALLACEA record (van Geel et al., 2011), transferred to the DeepCHALLA site using shared lithostratigraphy with mm-scale accuracy, and links between seismic-stratigraphic features registered at both sites and known near-global climate events back to 140 ka (Moernaut et al., 2010). Beyond 140 ka, the average sedimentation rate of the younger interval is linearly extrapolated to the base of the DeepCHALLA core sequence (Martin-Jones et al., 2020).

Lake Chala has been a deep crater lake throughout its history (Maituerdi et al., 2022), consequently the 214.8-meter long column of organic diatomaceous muds which accumulated in the past 250 kyr comprises only two distinct lithofacies (besides event deposits such as turbidites and tephra layers), namely mm-scale varve-like laminations and cm-scale banded sediments (Baxter et al., 2024). These lithofacies reflect different lake mixing regimes: mm-scale laminated sediments were deposited during periods of stable water-column stratification and permanent bottom-water anoxia (meromixis) as in Lake Chala today, whereas the occurrence of cm-scale banding suggests that the uppermost few cm of originally mm-scale laminated mud have been reworked by bottom currents associated with complete mixing events occurring at

intervals of once in several years to once in several decades. However, given the high temperature of the deep water in this tropical lake, the oxygen injected into it during such short-lived events must have been depleted rapidly (days rather than weeks) by bacterial activity (Lewis, 1987; De Crop and Verschuren, 2019) meaning that the lower water column was still in essence permanently anoxic. For display purposes, core sections with alternating mm-scale lamination and cm-scale banding, reflecting frequent transitions between episodes of stable and less stable meromixis, are assigned to a lithofacies type intermediate between the two main types (Baxter et al., 2023).

Analysis of high-resolution seismic profiles of the Chala basin penetrating to the start of lacustrine sedimentation c. 250 kyr ago (Moernaut et al., 2010; Maitituerdi et al., 2022) produced a reconstruction of past changes in lake depth to complement the DeepCHALLA lithostratigraphy which is primarily a reflection of changes in mixing regime. This seismic-stratigraphic sequence allowed definition of five major depositional stages in the history of Lake Chala (Stages V–I) that consist of either undisturbed and uniform basin-wide ('draped') sedimentation deposited under high lake-level conditions, or basin-focused ('ponded') sedimentation reflecting periods of low lake level. On the time scale covered by the DeepCHALLA sediment sequence, changes in lake level are related to both variation in lake water balance driven by changes in regional hydroclimate and to the long-term transformation of basin hydrology due to its continuous infilling by sediments.

Analysis of iso- and brGDGTs and various derived proxies in the DeepCHALLA sequence, supported by inferences from lithofacies distribution, the seismic lake-level record and fossil diatom assemblages, indicated that during the oldest depositional stages the water column of Lake Chala must have had a markedly different structure compared to today (Baxter et al., 2024). In particular the strong density gradient, which stabilizes the lower water column against complete mixing and leads to six distinct mixing zones in the modern lake system (Buckles et al., 2014) had not yet developed. This was likely due to the leaky nature of the lake at that time which allowed dissolved solids to be removed via subsurface outflow through the bottom and lower walls of the crater basin. Due to a series of lake-system changes occurring between c. 180–200 ka and c. 80 ka, chemical stratification became increasingly pronounced, with major influence on the niches available to brGDGT producers (van Bree et al., 2020; Baxter et al., 2021; Baxter et al., 2024). As a result, some GDGTs and derived proxies (e.g., crenarchaeol concentration, BIT index and IR_{6Me}) display strong ~23-kyr periodicity, as a reflection of the orbital insolation forcing of tropical climate, only from c. 180 ka onwards or later. Considering this evidence for the strong influence of lake-system changes on GDGT distributions during early lake history, the period during which these biomarkers may be used as climate proxies was conservatively constrained to the last ~160 kyr (Baxter et al., 2024).

3. Materials and methods

3.1. Sample preparation and analysis of brGMGTs

In the present study a total of 916 sediment horizons, previously analyzed for GDGTs (Baxter et al., 2024), were targeted for brGMGT analysis. Each sample is a 2-cm thick increment of mud extracted at a regular interval of 16 cm throughout the matrix sediments of the drilled DeepCHALLA sequence (i.e., skipping turbidites >2 cm thick) and also excluding samples which were later determined to consist of >25% turbidite material (Swai, 2018; Baxter et al., 2024). Sample preparation and analytical techniques were described previously (Baxter et al., 2023). In short, brGMGTs were analyzed using an Agilent 1260 Infinity ultrahigh performance liquid chromatography (UHPLC) system coupled to an Agilent 6130 single quadrupole mass detector according to the method of Hopmans et al. (2016). The brGMGTs were determined by their $[M + H]^+$ ions at m/z 1020, 1034 and 1048 and elute around 20 min later than brGDGTs containing one ring with the same molecular mass (i.e., Ib, IIb, IIIb and their isomers). To identify different brGMGTs and their isomers, peak retention times were compared to those of known brGMGTs (Baxter et al., 2019). Peak area integration was done using Agilent Masshunter and a detection threshold of 3×10^3 units was adopted; peak areas lower than this limit were excluded from proxy calculations. To calculate absolute abundances, the brGMGT peak areas were compared to the C_{46} glycerol trialkyl glycerol tetraether (GTGT) internal standard (m/z 744), assuming a comparable response of the mass spectrometer for all targeted compounds. The absolute concentrations of brGDGTs and brGMGTs were normalized to the amount of organic carbon present in the same 2-cm increment samples, determined at the University of Haifa, Israel (Baxter et al., 2024), and expressed as $\mu g\ g^{-1}\ C_{org}$. Due to a handful instances of missing sample weight or $\%C_{org}$ measurements, the time series of GDGT concentrations consist of $n = 909$ rather than $n = 916$ sediment horizons.

3.2. Numerical and statistical analysis

Principal component analysis (PCA) was carried out to investigate the relationships between brGMGTs and brGDGTs in DeepCHALLA sediments using the R statistical package FactoMineR (Le et al., 2008). PCA was performed on: 1) the fractional abundances relative to the full suite of brGDGTs and brGMGTs (22 compounds) and 2) the fractional abundances considering only the brGMGTs (7 compounds). In order to determine the impact of temporal variation in lake depth, mixing regime and water-column structure on the distribution of sedimentary brGMGTs, the proxies, concentrations, and PCA scores of the 916 samples (or 909 for the concentration time series) were grouped according to seismic depositional stage or type of lithofacies. The groups were compared by Tukey multiple comparison of means using a 95% family-wise confidence interval, where means are considered significantly different at the 5% level of significance. Data groupings summarized in boxplots or barplots are assigned letter labels to represent significantly different mean values; data groups which do not share any of the same letters are statistically different.

4. Results

4.1. BrGMGT concentrations and fractional abundances

All seven brGMGTs previously detected in surficial bottom sediments from 70 East African lakes (Baxter et al., 2019) and in three additional samples from Lake Chala (Baxter et al., 2021) were also present in all 916 analyzed core intervals of the DeepCHALLA sequence, and in similar concentrations: H1034b has the highest average fractional abundance (0.20), followed by H2010c (0.16), H1020b (0.13), H1048 (0.13), H1034c (0.13), H1020a (0.13) and H1034a (0.11) (Fig. 3). The summed concentration of all brGMGTs ranges between 2 and 220 $\mu g\ g^{-1}\ C_{org}$ (39 $\mu g\ g^{-1}\ C_{org}$ on average) and is characterized by large-scale swings in concentration between successive sediment horizons only 16 cm (~200 years) apart (Fig. 4c). Trends in brGMGT concentration follow a largely similar pattern as those of brGDGT concentration (Fig. 4d), reflected in strong positive correlation between them ($R = 0.83$, $p < 0.001$; Fig. 5a). Smoothed concentrations (the 10-point rolling averages, black curves in Fig. 4) also show substantial variation over longer timescales. Taking into account data hiatuses due to incomplete core recovery in the lower part of the sequence, brGMGT concentration (Fig. 4c) is fairly stable at below-average values during Stage I (20 $\mu g\ g^{-1}\ C_{org}$ on average), followed by a somewhat sharp increase at c. 205 ka, shortly after the start of Stage II. After this, brGMGT concentration generally increases towards a first prominent maximum dated to c. 155 ka. Between c. 145 ka and c. 80 ka, largely covering a long section of cm-scale banded sediments, brGMGT concentration is markedly lower, after which it steadily increases towards c. 60–45 ka, when highest values of the entire record are reached. This is followed by a general trend of decreasing

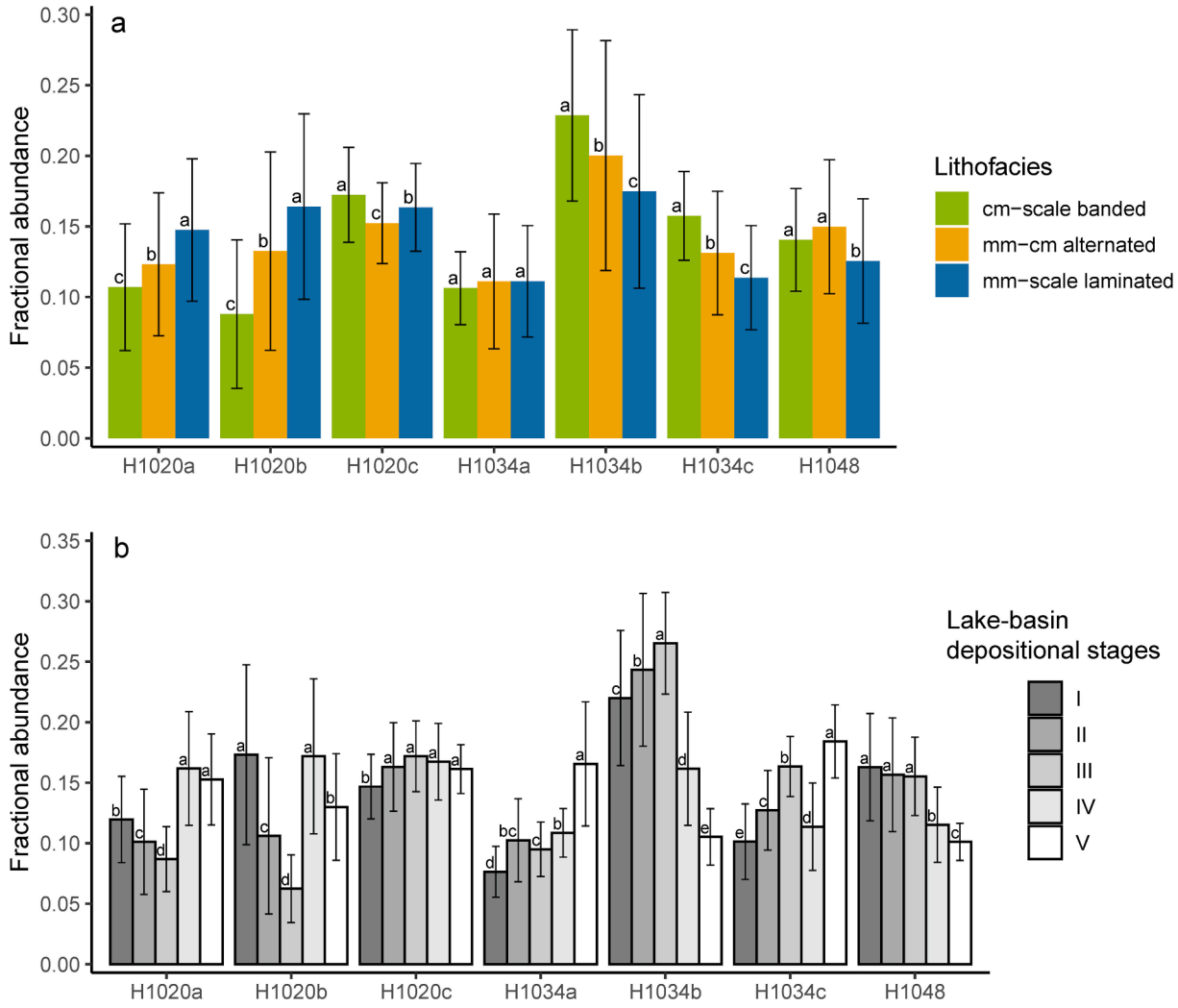

Fig. 3. Average fractional abundances of the seven brGMGTs detected in the DeepCHALLA sediment sequence with analyzed horizons grouped according to (a) lithofacies type and (b) lake-basin depositional stage, with whiskers in both panels representing one standard deviation around the mean. The depositional stages (I-V) refer to the five successive phases in lake-basin evolution as determined from seismic-stratigraphy data (Maitituerdi et al., 2022; Baxter et al., 2024); see also Fig. 4. Letters above the bars compare the mean values of the individual brGMGTs across lithofacies and depositional stage, respectively, using Tukey multiple comparison of means with a 95% family wise confidence interval; significantly different means are those that do not have any shared letters.

concentration from c. 45 ka until 12.8 ka, at which time brGMGT concentration increases sharply to the moderately high values characterizing the last 10 kyr.

BrGMGT concentrations measured in mm-scale laminated sediments (average $= 56\ \mu g\ g^{-1}\ C_{org}$) are significantly higher (95% confidence interval) than in cm-scale banded sediments (average $= 16\ \mu g\ g^{-1}\ C_{org}$), with samples from sediments with a mix of these two lithofacies having intermediate concentrations (average $= 31\ \mu g\ g^{-1}\ C_{org}$) (boxplots in Fig. 4c). Notably also the fractional abundances of all individual brGMGTs, except H1034a (which is the least common overall), differ significantly (95% confidence interval) between the two main lithofacies (Fig. 3a). In particular, average fractional abundances of H1020c, H1034b, H1034c and H1048 are elevated in cm-scale banded sediments compared to mm-scale laminated sediments, which instead contain relatively higher fractional abundances of H1020a and H1020b (Fig. 3a).

PCA of variation in the fractional abundances of brGMGTs in the DeepCHALLA sequence reveals that the first PC (PC1; 64.7% of the variance) is most strongly driven by the distributions of H1020a and H1020b opposed to those of H1034b and H1048 (Fig. 6a). Variation along PC2 (20.2% of the variance) largely relates to the contrasting distributions of H1034a and H1034c versus H1020b and H1034b. PC3 (6.9% of the variance) most strongly separates H1020c from all other brGMGTs (Fig. 6c). Considering the PCA of the fractional abundances of the full suite of seven brGMGTs and 15 brGDGTs (Fig. 6e), the brGMGTs mostly plot on the positive side of PC1 (56.4% of the variance) and the negative side of PC2 (14.8% of the variance). Along PC1 they cluster together with brGDGT Ia, IIa, and IIb, and along PC2 they cluster together with IIb and IIIa′, with the exception of H1034b which plots slightly positive on PC2. When the brGDGTs are included, only four brGMGTs (H1020a–c and H1034b) contribute more than 1% of the variance on either PC (Fig. 6d). In particular, H1034b behaves similar to IIa, whereas fractional abundances of the H1020a–c group match that of brGDGT IIb.

4.2. BrGMGT proxies

The range of %brGMGT values throughout the DeepCHALLA sequence is large (Fig. 7c), from 1.6 to 50.4% (19.3% on average), meaning that in some analyzed intervals brGMGTs are nearly as abundant as the brGDGTs. The %brGMGT generally decreases from the oldest sediments until c. 140 ka, interrupted by a few pronounced maxima, in particular at c. 230 ka. The period from c. 140 ka to 110 ka is characterized by large swings in %brGMGT, which fluctuates between < 15%

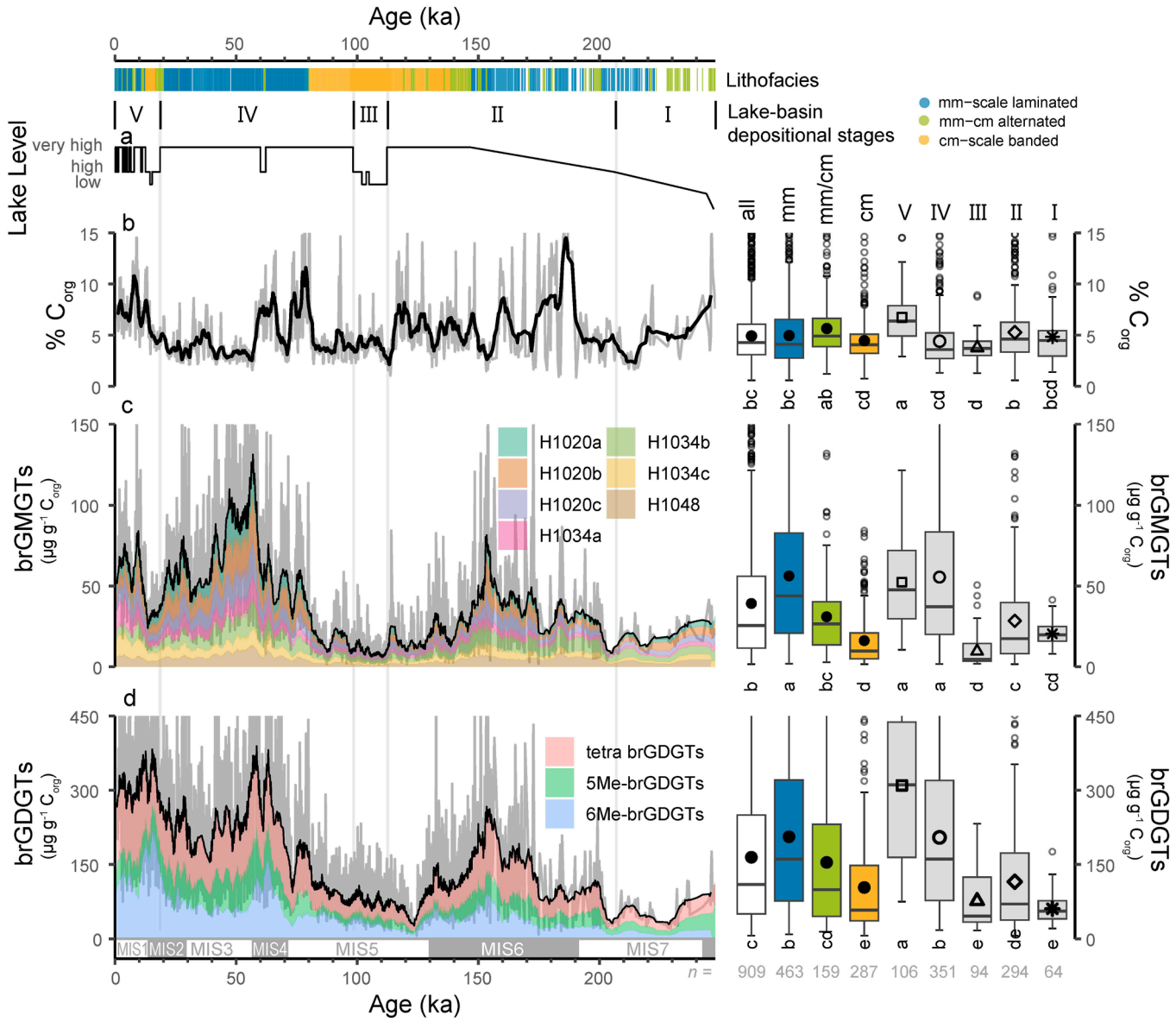

Fig. 4. Concentration profiles of brGMGTs and brGDGTs versus age in the 250-kyr DeepCHALLA sediment sequence. At the top, the lithofacies type of each sampled sediment horizon (colored bar; data hiatuses are due to incomplete core recovery in the lower part of the sequence), and the lake-basin depositional stages (I-V) based on seismic stratigraphy (Maitituerdi et al., 2022) are indicated. Panels show (a) the history of lake-level change reconstructed from seismic-reflection stratigraphy (Maitituerdi et al., 2022), (b) organic carbon content (%C_{org}; Baxter et al., 2024), and C_{org}-normalized concentrations of (c) brGMGTs (this study) and (d) brGDGTs (Baxter et al., 2024), with black curves representing 10-point rolling averages of the full data series shown in grey. The associated boxplots summarize the latter two records for all 909 analyzed intervals (white), according to lithofacies type (using the same color legend) and for each depositional stage I-V, indicating average values (solid or open symbols), median values (black line), the first and third quantiles (lower and upper hinges), whiskers (thin lines) extending to 1.5 × the interquartile range (IQR) from the hinges, and outliers (open circles) defined as data points beyond this range. Statistically significant groups of data were calculated using Tukey multiple comparison of means with a 95% family wise confidence interval and are indicated by letters underneath the box plots; significantly different means are those that do not have any shared letters. For improved visibility of temporal trends the y-axis of panels c and d (and associated boxplots) has been cropped, such that horizons with very high GDGT concentrations (and boxplot outliers) fall off-scale. For reference, the age scale below the plotted data also shows the timing of the marine isotope stages (MIS) as defined by Lisiecki and Raymo (2005).

and > 30%. Following this, %brGMGT is relatively low during the interval c. 110–97 ka (generally < 10%), largely overlapping with Stage III in lake-basin development. Other pronounced periods of fairly low % brGMGT values occur at c. 70–60 ka and 20–11 ka. Variation in % brGMGT is strongly correlated to the PC1 scores of the combined PCA on brGMGTs and brGDGTs ($R = 0.74$, $p < 0.001$; Fig. S1). Although comparison of %brGMGT with brGMGT and brGDGT concentrations (Fig. 5b–c) does not immediately reveal which group is the more dominant source of variability in the ratio between them, to a certain degree sediments with low %brGMGT values (e.g., < 15%) have low brGMGT concentrations (e.g., < 75 µg g^{-1} C_{org}) and those with the largest brGMGT concentrations (e.g., > 150 µg g^{-1} C_{org}) always have a %brGMGT value above 25% (Fig. 5b). This is reflected in the modest but significant correlation between %brGMGT and brGMGT concentration ($R = 0.33$, $p < 0.01$; Fig. S1), but not with brGDGT concentration ($R = 0.07$, $p > 0.01$), suggesting that the variability in brGMGTs is the dominant driver of this ratio.

The brGMGTI (Fig. 7d), a ratio between brGMGTs found to positively or negatively correlate with local MAAT in lake surface sediments (Baxter et al., 2019), ranges from 0.18 to 1 (0.69 on average), translating

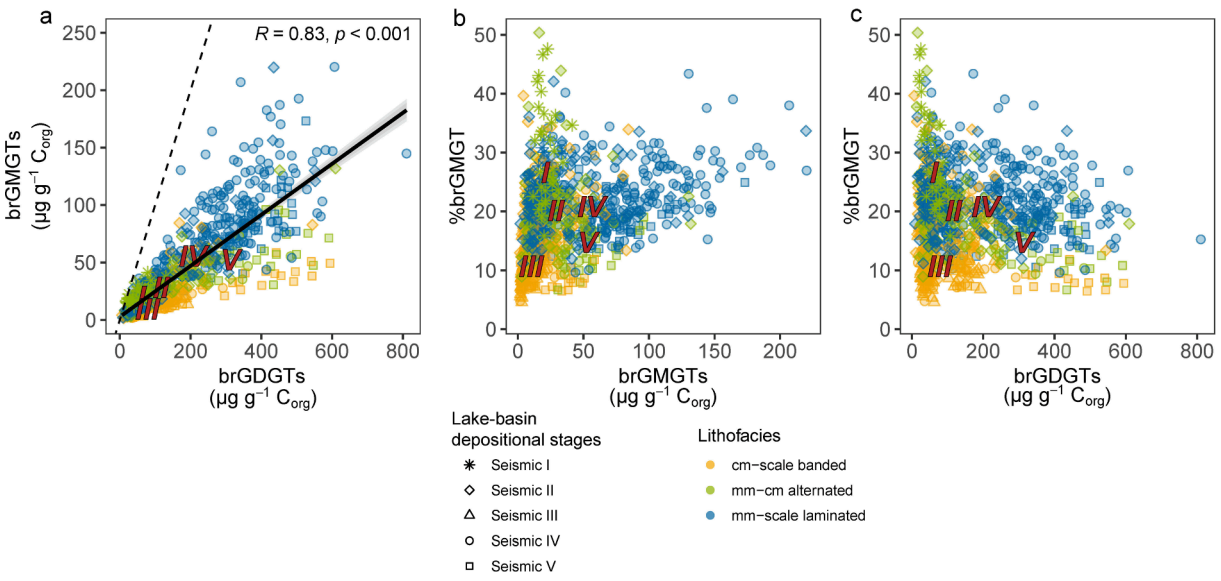

Fig. 5. Scatter plots of bacterial lipid data from 909 analysed intervals in the DeepCHALLA sediment sequence, labeled according to lake-development stage (symbols) and lithofacies (colors). (a) Comparison of C_{org} normalized brGMGT and brGDGT concentrations, with linear regression (solid line), uncertainty envelopes based on the 2nd and 3rd standard deviations (grey shading) and 1:1 relationship (dashed line); (b) %brGMGT versus brGMGT concentration; (c) %brGMGT versus brGDGT concentration.

into MAAT values between 7.7 and 29.5 °C, and a long-term average of 18.5 °C, when using the Baxter et al. (2019) East African lake calibration. Between c. 250 and c. 115 ka, brGMGTI displays a subtle but steadily increasing trend reaching peak values of up to ~0.9 (~28 °C) around 130 ka, overlain by short-term variability involving short-lived drops of magnitude 0.2 index value. After c. 115 ka, the brGMGTI baseline value is more stable at ~0.7 (~22 °C), before decreasing sharply at c. 80 ka, simultaneous with the sustained transition from cm-scale banded to mm-scale laminated sedimentation at that time. The period from c. 80 to 15 ka is characterized by relatively low brGMGTI values and inferred temperatures, which quickly rise thereafter. After a short-lived reversal to lower values between 11 ka and 9 ka, brGMGTI continues to rise to reach its highest values of the entire record near the top of the sequence. The brGMGTI displays many significant correlations with other derived variables, most strongly with PC2 of the PCA on brGMGT distribution ($R = 0.83$, $p < 0.001$; Fig. S1), which captures 20.2% of the variance. It also displays moderate negative correlation with %brGMGT ($R = -0.56$, $p < 0.001$).

MAAT estimates were also made using the SFS method of East African lakes brGMGT calibration (Baxter et al., 2019), and this yielded reconstructed temperatures ranging between 9.4 and 27.6 °C, with a long-term average of 24.8 °C (Fig. 7e). Between c. 250 and 180 ka, MAAT estimated by this method shows substantial short-term fluctuation but is mainly centered around a relatively low temperature of 20–22 °C. From c. 180 to 25 ka, larger and longer-duration temperature swings are inferred, often going below 18 °C and above 30 °C, followed by a 10-kyr long period of more sustained low MAAT (~22 °C). A sharp rise to 28 °C occurs at 15 ka, after which temperature remained close to this high value for the remainder of the time series. The SFS-based MAAT estimates correlate strongly with PC3 of the PCA on brGMGT distribution ($R = -0.72$, $p < 0.001$; Fig. S1), despite this PC explaining only 6.9% of the observed variance.

Analyzed samples that were extracted from mm-scale laminated sediments have significantly higher %brGMGT values (average = 22.0%) and lower brGMGTI values (average = 0.54, translating to MAAT of 16.9 °C), than those from cm-scale banded sediments (which have averages of 14.4% and 0.68, the latter translating to 20.1 °C; see boxplots in Fig. 7d-e). As can be expected, the %brGMGT and brGMGTI of samples reflecting a mixture of these two lithofacies have intermediate average values. On the other hand, SFS-based MAAT estimates on samples from mm-scale laminated and cm-scale banded sediments are not statistically different from one another (averages of 25.0 °C and 25.4 °C, respectively), while both are higher and statistically different (95% confidence interval) from those of samples from alternating mm- and cm-scale sedimentation (average = 23.4 °C) (Fig. 7d).

5. Discussion

5.1. Structural diversity of brGMGTs revealed by their contrasting distribution

Environmental interpretation of the distributional variation among individual brGMGTs in lake sediments and other settings would be assisted if their exact chemical structures had already been elucidated, however this awaits time-consuming efforts, including isolation and application of advanced techniques such as two-dimensional NMR. Nevertheless, distributional variation among brGMGTs in the 250-kyr DeepCHALLA sequence provides tentative insights. To start, considering the combined PCA of brGMGTs and brGDGTs, the former plot on the positive side of PC1 along with brGDGT Ia and IIa, and opposite of the negatively scoring IIa′, IIIa′ and IIb′ (Fig. 6e). Therefore, as PC1 appears to reflect the differing behaviour of 5-methyl versus 6-methyl brGDGT isomers, this distribution can be interpreted to suggest that the most abundant brGMGT, H1034b, possesses an additional methyl group at the 5th and not the 6th carbon number position. Considering the PCA of brGMGTs only (Fig. 6a and c), the contrasting scores of H1034a and H1034c versus H1034b and other brGMGTs along PC2, which drives 20.2% of the observed variance, suggests that H1034a/c may in fact be 6-Me isomers. H1048a, on the other hand, behaves similarly to H1034b in scoring positively along PC1 and negatively along PC2 (which together explain 85% of the variance), suggesting that also H1048 contains two C-5 methyl groups. Therefore, PC1 (explaining 64.7% of the variance) appears to relate to the brGMGTs' degree of methylation at C-5, mainly separating H1034b and H1048 (with respectively 3 and 4 methyl substituents) from H1020a and H1020b (with only two methyl substituents). Although PC3 only explains 6.9% of the variation in brGMGT distribution, it is clearly determined by the fractional abundance of H1020c (Fig. 6c). This contrasting behaviour of the three H1020 isomers in the DeepCHALLA record suggests that they are favoured by different ecological conditions.

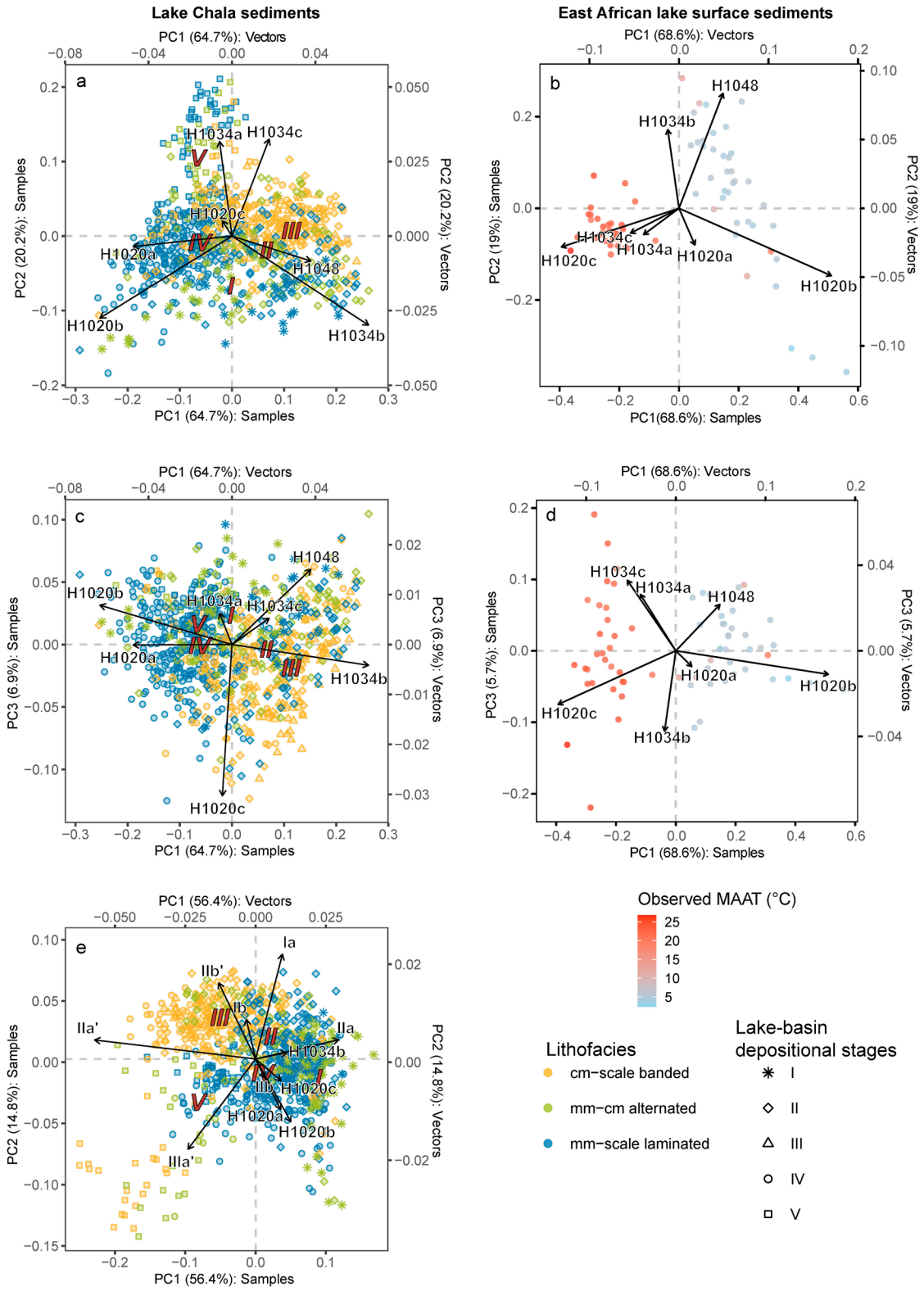

Fig. 6. PCAs of brGMGT distribution in DeepCHALLA sediments (a,c,e) and in surficial bottom sediments of the East African lake dataset used in the calibration of Baxter et al. (2019) (b,d). Panels show PC1 versus PC2 (a,b) and PC1 versus PC3 (c,d) of PCAs on brGMGT fractional abundances, and PC1 versus PC2 of the PCA on the fractional abundances of the full suite of brGMGTs and brGDGTs in DeepCHALLA sediments (e). Individual brGMGTs or brGDGTs that contribute < 1% to variance in the data on either plotted PC were included in the analyses but not displayed in the plots to improve readability. In PCA of the full suite of brGMGTs and brGDGTs in the East African lake dataset (not shown), no brGMGTs contributed more than 1% to the variance along either PC1 or PC2. For DeepCHALLA sediments, individual samples are labeled according to lake-basin depositional stage (symbol) and lithofacies (color). Red numerals (I-V) represent the average PC scores (or centroid values) of DeepCHALLA sediment horizons sorted according to depositional stage. Separate PC axes are provided for the position of the GDGT vectors (top and right) and individual sediment samples (left and bottom).

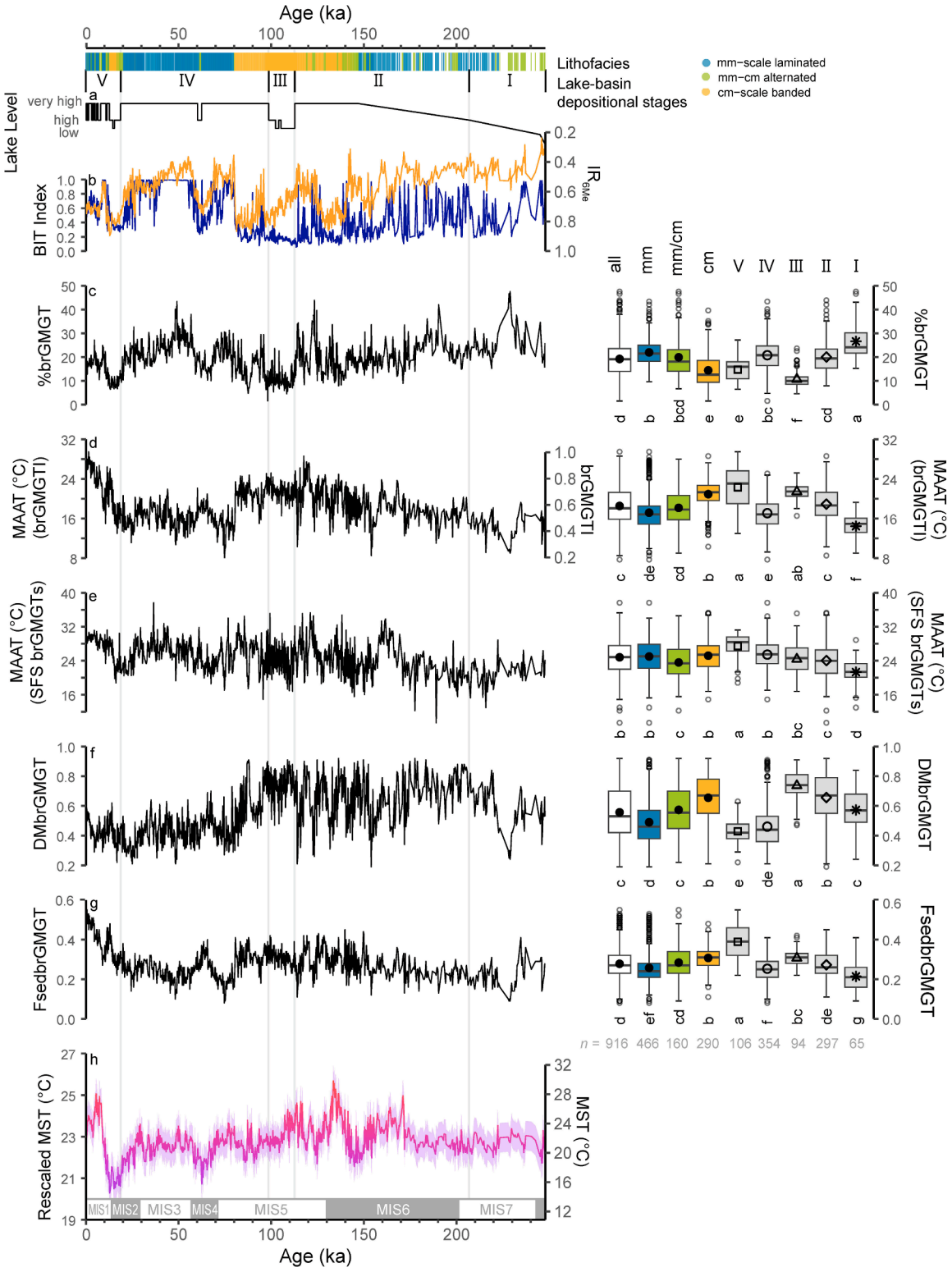

Fig. 7. Application of brGMGT- and brGDGT-based paleoclimate proxies to the 250-kyr DeepCHALLA sediment sequence. At the top, the lithofacies type of each sampled sediment horizon (colored bar; data hiatuses are due to incomplete core recovery in the lower part of the sequence), and the basin-development stages (I-V) based on seismic stratigraphy (Maitituerdi et al., 2022) are indicated. Panel (a) shows the history of lake-level change reconstructed from seismic-reflection stratigraphy (Maitituerdi et al., 2022). The following panels show (b) the BIT index (dark blue) and IR_{6Me} (orange) (Baxter et al., 2024), (c) %brGMGT, MAAT estimates based on (d) brGMGTI and (e) the relative abundance of brGMGTs selected using stepwise forward selection (SFS), the (f) DMbrGMGT and (g) FsedbrGMGT indices defined here based on the behaviour of brGMGTs in DeepCHALLA sediments as revealed by PCA, and (h) Mean Summer Temperature (MST) calculated according to the brGDGT-based calibration of Pearson et al. (2011), rescaled using an ensemble reconstruction of temperature records from seven other East African lakes (Baxter et al., 2023), as previously presented by Baxter et al. (2024).

5.2. Niches of brGMGT producers in Lake Chala

The much higher %brGMGT and markedly different distribution of brGMGTs in three surficial bottom sediments (integrating the last ~30 years of sedimentation; Verschuren et al., 2009; van Geel et al., 2011) from that in the water column (SPM and settling particles) and surrounding catchment soils led Baxter et al. (2021) to the conclusion that the majority of brGMGT production occurs within the sediments. Although brGMGTs were detected in SPM from the anoxic deepwater zone (almost exclusively H1020a–c and H1034b), production within the water column was considered to contribute much less to the sedimentary pool. Specifically, only H1020a and H1020b were considered to originate substantially from aquatic production as their fractional abundance is higher in the modern water column than in surficial bottom sediments. Over the entire DeepCHALLA record analysed here, Lake Chala sediments on average contain near-equal amounts of the seven detected brGMGTs, comparable to their distribution in surficial bottom sediments (Fig. 2; Baxter et al., 2021) except that the DeepCHALLA sediments generally have higher fractional abundances of H1020a and H1020b (Fig. 2 and 3). This difference can be explained by the greater environmental variability covered by 250 kyr of sedimentation; indeed, there are time windows in the DeepCHALLA sequence when brGMGT distributions more closely resemble those in surficial (modern) profundal bottom sediments (Fig. 3b).

As predicted by the percentages recorded in surficial bottom sediments (Baxter et al., 2021), also DeepCHALLA sediments have a much higher %brGMGT on average (19%, range 2–5%) than modern-day settling particles or SPM (2%, range 0–8%). Therefore, at first glance the brGMGT distributions in the DeepCHALLA sediments appear to support a mainly sedimentary origin. On the other hand, a more detailed appraisal of the trends and variability of brGMGTs in the DeepCHALLA record points toward a more complex explanation surrounding their primary niche and ecological significance in this meromictic tropical crater lake. First and foremost, down-core variability in the concentrations and distributional pattern of brGMGTs and brGDGTs in the DeepCHALLA sequence is not a consequence of differential post-burial preservation of certain lipids related to varying oxygen exposure of the lake bottom. Namely, considering changes in sediment lithology to reflect differences in the frequency of bottom water oxygenation, cm-scale banded sediments do not contain significantly lower $\%C_{org}$ than mm-scale laminated sediments (Fig. 4b), as would be predicted if increased oxygen exposure associated with intermittent deep mixing meaningfully reduced the preservation of settling organic material before permanent burial. This supports the idea that oxygen injected to the lower water column during occasional complete mixing events was depleted rapidly (De Crop and Verschuren, 2019) such that the bottom environment of Lake Chala can be considered permanently anoxic even across cm-scale banded sections. Lesser stability of brGMGTs and brGDGTs relative to average bulk organic matter is unlikely (Huguet et al., 2008). Second, the molecular structure of brGMGTs and brGDGTs is similar in that the most labile bonds in both groups are the four ether bonds, inferring similar stability and degradation rates. Therefore, also differential preservation of compounds within these two groups is unlikely (Schouten et al., 2013). Lack of a clear influence of oxygen exposure on the distribution of brGMGTs and brGDGTs in the DeepCHALLA record is well illustrated by opposing PC scores for the three periods of mm-scale banded sedimentation in Stages I-II, Stage IV and Stage V, revealing widely different distributional patterns (see blue points in Fig. 6a). We, therefore, attribute downcore changes in the abundance and relative proportion of brGMGT and brGDGTs to variations in the proliferation of their respective producers.

Strong correlation between brGMGT and brGDGT concentrations throughout the sediment sequence ($R = 0.83$, $p < 0.001$; Fig. 5a) suggests that these membrane lipids are either produced by the same (groups of) bacteria or by species with largely overlapping ecological niches. However, in contrast to the presumed sedimentary production of brGMGTs, the primary source of brGDGTs in Lake Chala sediments appears to be the anoxic lower water column (van Bree et al., 2020; Baxter et al., 2024). Moreover, the concentrations of these two groups show greater coupling (i.e., plotting closer to the 1:1 line in Fig. 5a) and are more strongly correlated ($R = 0.86$ versus $R = 0.75$; $p < 0.001$ for both cases) in mm-scale laminated sediments than in cm-scale banded sediments, suggesting that differences in lake mixing impact the relationship between these two groups. Namely, a taller anoxic water column setting suggested by mm-scale lamination appears to increase the overlap between the niches of brGMGT and brGDGT producers.

The range of %brGMGT values (2–50%) in the DeepCHALLA record, i.e., variation in the proportion of brGMGTs and brGDGTs through time, is larger than those observed in globally distributed peats (0–20%; Naafs et al., 2018) and in surficial sediments from East African lakes (0–31%; Baxter et al., 2019), where %brGMGT values increase with increasing mean annual air temperature. This large range is particularly striking considering the near-permanent anoxia of Lake Chala's lower water column throughout its 250-kyr history (Baxter et al., 2024). Detailed studies of brGDGTs in the water column and sediment record of Lake Chala showed that fluctuations in lake depth and mixing exert important influence on brGDGT concentrations and proxies (van Bree et al., 2020; Baxter et al., 2024). It is therefore highly likely that also %brGMGT is influenced by changes in these parameters in the past. For instance, assuming exclusively aquatic and sedimentary sources for brGDGTs and brGMGTs, respectively, %brGMGT would be expected to increase when lake depth is reduced, because reduction in overall height of the anoxic zone will decrease the relative abundance of brGDGTs. However, in the DeepCHALLA record, brGDGT concentrations do not appear to drive differences in %brGMGT, whereas brGMGT concentrations do show a clear influence (Fig. 5b–c; Fig. S1), arguing against this simple dichotomy in sources. Moreover, %brGMGT is correlated with the BIT index ($R = -0.61$, $p < 0.001$) and isomer ratio (IR_{6Me}; $R = 0.52$, $p < 0.001$) (Fig. S1), which in Lake Chala both relate to past changes in moisture balance (Baxter et al., 2021; Baxter et al., 2024). The similarities between the time series of these proxies appear particularly strong in the last 110 kyr (Fig 7b-c). For example, %brGMGT was very low (often < 10%) during the intervals c. 110–97 ka and 20–12 ka, known episodes of greatly reduced/decreasing lake level inferred from seismic reflection data (i.e., the prolonged low-stands during Stage III and the first half of Stage V; Maitituerdi et al., 2022 and Fig. 7), and also evident in the time series of the BIT index and IR_{6Me}.

The combined data indicate that %brGMGT is mostly influenced by lake level or mixing changes and not temperature, but that its variability is not in the expected direction if the brGMGTs were produced mostly within the bottom sediments. Increased concentrations of both brGMGTs and brGDGTs during periods of high lake level and/or stable meromixis (Fig. 4) indicate that both benefit from expansion of a shared niche of brGDGT and brGMGT producers in the anoxic lower water column, although their response appears to be disproportionate such that %brGMGT increases with rising lake level due to a greater relative abundance of brGMGTs in the water column. Altogether, this strongly suggests that aquatic production contributes a greater proportion of brGMGTs to the sedimentary pool in Lake Chala than was previously estimated (Baxter et al., 2021).

Adding to this discussion, in PCA of the fractional abundances of the full suite of brGMGTs and brGDGTs in the DeepCHALLA record brGMGTs cluster together largely within the second quadrant (positive PC1, negative PC2; Fig. 6e), indicating that variation in their distributions is more restricted than that of brGDGTs. This might suggest that brGMGTs in Lake Chala are produced by the same (groups of) bacteria or by bacteria with a shared ecological niche, but that this microbial community has considerably more limited taxonomic or ecological range than the brGDGTs producers. However, although all brGMGTs behave similarly, only brGMGTs H1020a–c and H1034b contribute more than 1% of the variance to either PC1 or PC2 when the brGDGTs are included in the analysis, and mainly group with the 5-Me isomers

(IIa and IIb) and Ia which also score positively on PC1 (Fig. 6e). As all brGMGTs have comparable average fractional abundances in the DeepCHALLA record (Figs. 2 and 3), this would suggest that the variability of the brGMGTs that do not contribute meaningfully to the variance (H1034a, H1034c and H1048) are responsive to different ecological drivers. In Lake Chala, 5-Me brGDGTs are mostly produced in the part of the anoxic zone directly below the oxycline (van Bree et al., 2020), which is transient in nature and largely annihilated during the mixing season when enhanced upper water-column mixing expands the upper oxygenated layer (Buckles et al., 2014; Baxter et al., 2024). This might suggest that also the producers of H1020a–c and H1034b are more susceptible to variation in water column stability than those of the other GMGTs. Indeed, also in the modern lake system H1020a–c and H1034b are found widely throughout the anoxic water column, whereas H1034a, H1034c and H1048 are relatively scarce in space and in time, appearing only sporadically and then almost exclusively in the permanently stratified lower water column at depths equal to or exceeding 60 m (Baxter et al., 2021). Taken together, these results suggest that brGMGTs H1034a, H1034c and H1048 in Lake Chala are more singularly produced within (recently deposited) bottom sediments, whereas H1020a–c and H1034b derive to greater extent from aquatic production. This dichotomy is clearly visible in the PCA of brGMGT distribution in the DeepCHALLA record (Figs. 6a), where the negative PC2 scores of H1020b and H1034b contrast with the positive PC2 scores of H034a and H1034c. The dominant source of H1048 remains somewhat unclear, because its occurrence in the modern system seemed to point to production in the sediment (Baxter et al., 2021) whereas in the PCA of DeepCHALLA sediments it aligns with the presumably aquatically produced H1034b.

Based on these associations, we propose that the balance between these two groups of brGMGTs might be used to express the temporally varying contribution of aquatic and sedimentary sources to brGMGTs in the DeepCHALLA sediment sequence. Although 100% sedimentary or aquatic production of either group is unlikely, we here define the FsedbrGMGT (fraction of sedimentary brGMGTs) index as reflecting the relative contribution of sedimentary production on a scale from 0 to 1:

$$FsedbrGMGT = \frac{(H1034a + H1034c)}{(H1020a + H1020b + H1020c + H1034a + H1034b + H1034c)} \quad (5)$$

As such, the FsedbrGMGT index of individual sediment horizons in the DeepCHALLA sequence is strongly correlated to PC2 of the PCA on brGMGT distribution ($R = 0.99$, $p < 0.001$; Fig. S1). In monthly depth profiles of SPM from the modern Lake Chala, FsedbrGMGT is, as expected, close to zero throughout most of the year (Fig. 8a), given the mainly anaerobic aquatic source of the brGMGTs found in SPM. However, during the deep-mixing season values up to 0.4 are observed both directly above the oxycline and in the lowermost water column (70 m and below). As brGMGT concentrations are very low throughout the upper 50 m of the water column during deep mixing (Baxter et al., 2021; Fig. 8c), it is difficult to assess if the higher FsedbrGMGT values are meaningful or rather an artefact of these low abundances. On the other hand, occasionally elevated FsedbrGMGT values in the lower water column may reflect a notable contribution of brGMGTs which have been resuspended from the bottom sediments. In the DeepCHALLA sediments, this ratio indicates that the average contribution of brGMGTs from sedimentary production throughout the sequence may have been close to ~30% (Fig. 7g). With the exception of a ~10-kyr period of increased contribution from aquatic sources centered at c. 225 ka, FsedbrGMGT fluctuates around an average value of 0.2 from the base of the record until c. 150 ka, at which point the baseline of this variability slightly increases to 0.3 and then stays at this level until c. 80 ka. The supposedly higher contribution of sedimentary brGMGTs from c. 150 ka onward suggests an overall lower lake level or more deeply mixed water column. This is supported by the more common occurrence of cm-scale banded sedimentation during c. 150–80 ka, although a clear additional response to the Stage III low-stand, as seen in the moisture balance proxies (BIT index and IR_{6Me}), is not visible. After c. 80 ka, a greater degree of long-term variability in the inferred contribution between aquatic and sedimentary sources develops, with FsedbrGMGT displaying a somewhat anti-phased relationship with the BIT index and IR_{6Me}, reflecting the expected connection between an overall taller (thinner) anoxic water column and higher (lower) aquatic brGMGT contribution. The fact that

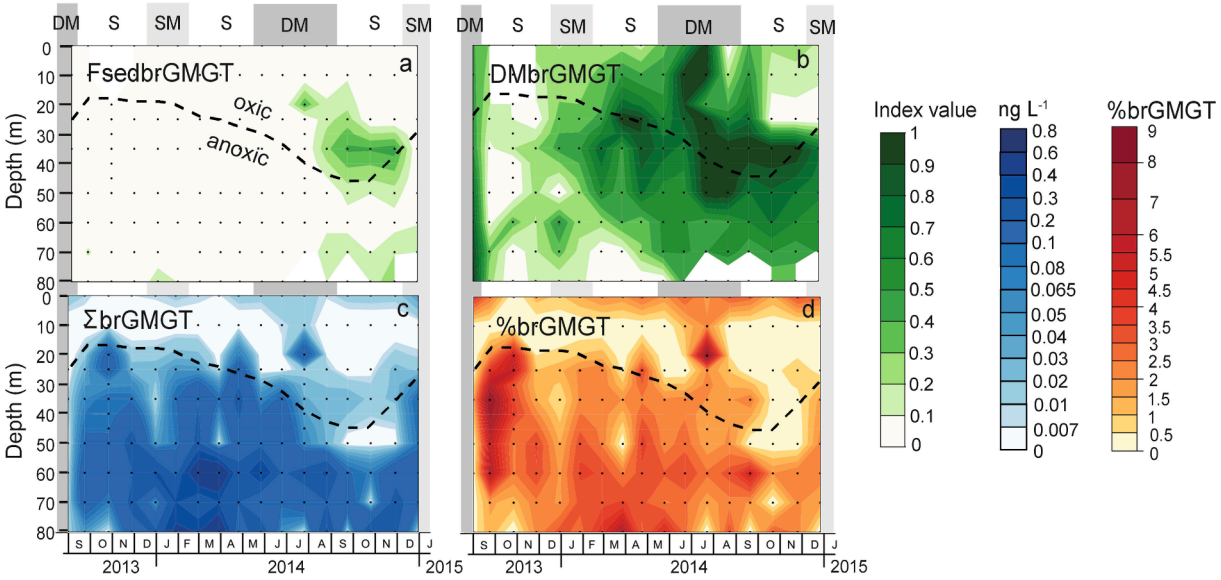

Fig. 8. Interpolated values of the FsedbrGMGT (a) and DMbrGMGT (b) indices, as defined in Eqs. 5 and 6, in suspended particulate matter (SPM) collected monthly from September 2013 to January 2015 throughout the water column of Lake Chala. Pure white areas reflect instances where these indices are undefined due to the absence brGMGTs which constitute the denominator of the given ratios. The summed total concentrations (in ng L^{-1}) of the seven known brGMGTs (c) and %brGMGT in the same SPM dataset (d), both from Baxter et al. (2021) are shown for reference. Black points represent the sampling depths/months analyzed, grey background shading shows the timing of seasonal shallow (SM) and deep mixing (DM) of the water column, and the overlying dashed black line traces oxycline depth (van Bree et al., 2018).

lake moisture balance only appears to influence brGMGT sources in the last c. 80 ka may in fact suggest that the association of individual brGMGTs with particular ecological niches has shifted over time. This shift may partly relate to the developing chemical gradient in Lake Chala (Baxter et al., 2024) and its potential influence on the niche(s) of brGMGT producers. Indeed, although mean fractional abundances of the individual brGMGTs are significantly different (95% confidence interval) between mm-scale laminated sediments and cm-scale banded sediments (Fig. 3a), it is clear that their variability through time is more prominent (Fig. 6a and 3b).

5.3. Potential of brGMGT distribution as paleotemperature proxy

Application of brGMGTI and SFS calibrations, based on relationships in the 70-site dataset of East African lakes (Baxter et al., 2019), to surficial bottom sediments of Lake Chala resulted in estimates of MAAT that matched modern-day temperature (Baxter et al., 2021; Fig. S2b–c). However, application of these two calibrations to the 250-kyr DeepCHALLA sequence yields markedly different reconstructions of past temperature change (Figs. 7d–e). Neither of the two MAAT reconstructions shows strong resemblance to the succession of marine isotope stages, except that brGMGTI correctly estimates below-average temperature during the last glacial period (MIS4–MIS2) and both methods reconstruct increasing MAAT in the last c. 15 kyr, i.e. during the last deglaciation and current interglacial period. However, the range of inferred MAAT values is questionably large, with deglacial warming of ~10 °C and ~14 °C, respectively, estimated by SFS calibration and brGMGTI. Moreover, both MAAT time series include temperature swings exceeding 8 °C within a few hundred years, which must be considered unrealistic for this equatorial site.

Like the FsedbrGMGT index, brGMGTI is strongly related to PC2 of the PCA of the brGMGTs ($R = 0.83$, $p < 0.001$), which accounts for 20.2% of the variance in sedimentary brGMGT distribution (Fig. S1). Consequently, brGMGTI is also strongly correlated to the FsedbrGMGT index ($R = 0.85$, $p < 0.001$), suggesting that fluctuations between sedimentary and aquatic sources of brGMGTs may overprint a possible temperature signal contained in brGMGTI. MAAT reconstructed using the SFS calibration, on the other hand, is strongly correlated to PC3 ($R = -0.67$, $p < 0.001$) but this PC explains only 6.9% of the observed variance in sedimentary brGMGT distribution. Hence, although these two methods both capture aspects of brGMGT variability, their temperature functions explain a different part of brGMGT variability, and neither of them is strongly tied to the most important component of the variance as expressed along PC1 (which covers 64.7% of the variance). Additionally, neither time series is compatible with the brGDGT-based MST record based on the calibration of Pearson et al. (2011), which after careful review of all available modern-system data and alternative iso- and brGDGT-based calibrations (e.g., methods using TEX_{86} or MBT'_{5me}), has been concluded to be the most reliable method for temperature reconstruction at Lake Chala (Baxter et al., 2023; Baxter et al., 2024). Notably, MST does not correlate significantly to PC3 of brGMGT distribution ($R = -0.28$, $p > 0.01$; Fig. S1), suggesting that temperature is not a major driver of variability among individual brGMGTs throughout the DeepCHALLA record.

In this context, attention is drawn to the observation that variability among brGMGTs registered in the DeepCHALLA record differs markedly from that in the East African lakes calibration dataset, where the brGMGTI-inferred MAAT gradient is clearly expressed along PC1 (Fig. 6b,d). As discussed earlier, in the case of Lake Chala sediments, the PC1 of brGMGT distribution, which explains almost two-thirds (~65%) of the variance, is strongly correlated ($R = 0.99$, $p < 0.001$; Fig. 6a) a) to the degree of brGMGT methylation, expressed by the here defined DMbrGMGT index:

$$DMbrGMGT = \frac{(H1034b + H1048)}{(H1020a + H1020b + H1034b + H1048)} \quad (6)$$

Considering that for brGDGTs from diverse settings the degree of methylation at C-5 is negatively correlated to temperature (e.g., De Jonge et al., 2014; Raberg et al., 2022) a similar relationship might also be expected for brGMGTs. Indeed, the degree of methylation of brGMGTs in peats, calculated using an index (i.e., $H\text{-}MBT_{acyclic}$) designed for their more limited structural diversity in that setting, has been found to follow the trends in methylation of regular brGDGTs in the globally distributed peat dataset (Naafs et al., 2018). However, the DMbrGMGT index of SPM from Lake Chala covers the full range of possible values (0–1; Fig. 8b), although measured temperature of the water column varied only between 22°C and 26°C across depth and over the annual cycle (van Bree et al., 2018). Expectedly therefore, variability in the DMbrGMGT index throughout the DeepCHALLA sequence (Fig. 7g) does not show a clear relationship with the MST reconstruction. The index displays a dramatic baseline change from high (~0.8) to lower values (~0.4) at c. 80 ka, occurring when the BIT index and IR_{6Me} indicate a rapid increase in moisture balance, and the transition from cm-scale banded to mm-scale laminated sediments suggests more stably stratified water column conditions. Therefore, although the influence of water column dynamics on DMbrGMGT is apparent, the more precise environmental significance of these changes and their relationship with the brGMGT distributions in Lake Chala is as yet difficult to determine. Overall, neither of the calibration methods introduced following analysis of brGMGT distribution in the East African lake dataset or ratios reflecting important aspects of brGMGT variability in Lake Chala sediments result in reconstructions appearing to track past temperature change when applied to the DeepCHALLA sequence. This poor performance may relate to the scarcity of intermediate-temperature (i.e., mid-elevation) lakes in the East African lake dataset, and more specifically deep meromictic lakes at middle or high elevations which can credibly serve as analogs for Lake Chala during past glacial episodes (Fig. S2; Baxter et al., 2024). Consequently it remains unclear whether the linear relationships between brGMGT distribution and MAAT represented by the mainly shallow lakes in the calibration dataset also hold for deep lakes.

6. Conclusions

BrGMGTs constitute a large proportion of bacterial membrane-spanning ether lipids extracted from Lake Chala sediments, with H2010a–c and H1034b likely produced predominantly in the water column whereas H1034a and H1034c are predominantly produced in recently deposited bottom sediments. As expected, the ratio between these two groups, newly defined here as the FsedbrGMGT index, is responsive to past changes in lake level, but most clearly during the last 80 ka, suggesting that the local ecological niche of brGMGT producers may have shifted over time, prompted by increasingly pronounced chemical water-column stratification. Although initial studies in East African lakes suggested that the %brGMGT may be partially related to air temperature, in Lake Chala this appears to be (indirectly) controlled by changes in lake depth at least during the last c. 110 ka, when the comparability of the ratio to the BIT index, IR_{6Me}, and seismic reflection-based lake level record is enhanced. Although higher concentrations of both brGDGTs and brGMGTs result from greater lake depth, this influence appears to disproportionately affect the brGMGT producers, leading to an overall increase in %brGMGT when the anoxic zone is expanded. Application of brGMGTI and SFS-based temperature inference models calibrated using surface sediments from 70 East African lakes resulted in dissimilar MAAT reconstructions, which both appear unrealistic due to their lack of response to global temperature trends, improbably large temperature range, and dramatic short-term swings in temperature. This may be related to the lack of deep, permanently stratified lakes from higher elevations (i.e., cooler climate regimes) in the East African lake dataset. Therefore, the brGDGT-derived MST reconstruction based on the lake calibration by Pearson et al. (2011)

remains the most trustworthy method for reconstructing past temperature history from the sediments of Lake Chala. Regardless, the present study has greatly increased our understanding of the occurrence and relative distributions of brGMGTs in lacustrine sediments. Further research should focus on identifying their precise producers and ecological niches in lakes and other contexts. These results highlight a recurrent issue when using empirical calibrations based on surficial bottom sediments from modern-day lakes to predict past environmental variability: agreement of the model-derived proxy signal recorded in the surface sediments of individual lakes with observed local temperature does not ensure that down-core application at that particular site will be successful. Additional research, such as detailed modern-system investigations and multi-proxy validation studies, should be pursued before applying climate-proxy calibrations to the local sediment record.

Declaration of Competing Interest

The authors declare that they have no known competing financial interests or personal relationships that could have appeared to influence the work reported in this paper.

Data availability

Data associated with this article is available via Zenodo: https://zenodo.org/records/10998953.

Acknowledgements

This research was mainly co-financed by NESSC Gravitation Grant 024.002.001 from the Dutch Ministry of Education, Culture and Science (OCW) to JSSD; and by Hercules infrastructure grant AUGE/15/14-G0H2916N from the Research Foundation of Flanders and a Francqui research professor mandate to DV. Recovery of the Lake Chala sediment record was accomplished with support of ICDP through the DeepCHALLA project (https://www.icdp-online.org/projects/world/africa/lake-challa/), and facilitated by the government of Kenya through permit P/16/7890/10400 from the National Commission for Science, Technology and Innovation (NACOSTI) and license EIA/PSL/3851 from the National Environmental Management Authority (NEMA); and by the government of Tanzania through permits NA-2016–67 (270–285) and NA-2016–201 (277–292) from the Tanzania Commission for Science and Technology (COSTECH) and permit EIA/10/0143/V.I/04 from the National Environmental Management Council. The authors wish to thank DeepCHALLA partners and their institutions in Kenya and Tanzania for project facilitation; Caxton M. Oluseno and the Kamba and Taveta communities of Lake Chala area for field assistance; and the National Lacustrine Core Facility (LacCore) at the University of Minnesota (USA) for organizing the splitting, logging and initial processing of core samples. We are further grateful to J. Riekenberg and A. Mets for analysis of samples. We kindly thank the associate editor, I. Castañeda, and reviewers Z. Zeng and D. Naafs whose feedback has improved this manuscript.

Appendix A. Supplementary material

Supplementary data associated with this article can be found, in the online version, at https://doi.org/10.1016/j.orggeochem.2024.104812.

References

Barker, P.A., Hurrell, E.R., Leng, M.J., Wolff, C., Cocquyt, C., Sloane, H.J., Verschuren, D., 2011. Seasonality in equatorial climate over the past 25 k.y. Revealed by oxygen isotope records from Kilimanjaro. Geology 39, 1111–1114. https://doi.org/10.1130/G32419.1.

Bauersachs, T., Schwark, L., 2016. Glycerol monoalkanediol diethers: A novel series of archaeal lipids detected in hydrothermal environments. Rapid Communications in Mass Spectrometry 30, 54–60. https://doi.org/10.1002/rcm.7417.

Baxter, A.J., van Bree, L., Peterse, F., Hopmans, E.C., Villanueva, L., Verschuren, D., Sinninghe Damsté, J.S., 2021. Seasonal and multi-annual variation in the abundance of isoprenoid GDGT membrane lipids and their producers in the water column of a meromictic equatorial crater lake (Lake Chala, East Africa). Quaternary Science Reviews 273, 107263. https://doi.org/10.1016/j.quascirev.2021.107263.

Baxter, A.J., Hopmans, E.C., Russell, J.M., Sinninghe Damsté, J.S., 2019. Bacterial GMGTs in East African lake sediments: Their potential as palaeotemperature indicators. Geochimica et Cosmochimica Acta 259, 155–169. https://doi.org/10.1016/j.gca.2019.05.039.

Baxter, A.J., Peterse, F., Verschuren, D., Sinninghe Damsté, J.S., 2021. Anoxic in situ production of bacterial GMGTs in the water column and surficial bottom sediments of a meromictic tropical crater lake: Implications for lake paleothermometry. Geochimica et Cosmochimica Acta 306, 171–188. https://doi.org/10.1016/j.gca.2021.05.015.

Baxter, A.J., Verschuren, D., Peterse, F., Miralles, D.G., Martin-Jones, C.M., Maitituerdi, A., Van der Meeren, T., Van Daele, M., Lane, C.S., Haug, G.H., Olago, D. O., Sinninghe Damsté, J.S., 2023. Reversed Holocene temperature–moisture relationship in the Horn of Africa. Nature 620, 336–343. https://doi.org/10.1038/s41586-023-06272-5.

Baxter, A. J., Peterse, F., Verschuren, D., Maitituerdi, A., Waldmann, N., Sinninghe Damsté, J. S., 2024. Disentangling influences of climate variability and lake-system evolution on climate proxies derived from isoprenoid and branched glycerol dialkyl glycerol tetraethers (GDGTs): the 250 kyr Lake Chala record, Biogeosciences, 21, 2877-2908. https://doi.org/10.5194/bg-21-2877-2024.

Bijl, P.K., Frieling, J., Cramwinckel, M.J., Boschman, C., Sluijs, A., Peterse, F., 2021. Maastrichtian-Rupelian paleoclimates in the southwest Pacific - A critical re-evaluation of biomarker paleothermometry and dinoflagellate cyst paleoecology at Ocean Drilling Program Site 1172. Climate of the Past 17, 2393–2425. https://doi.org/10.5194/cp-17-2393-2021.

Blaga, C.I., Reichart, G.J., Heiri, O., Sinninghe Damsté, J.S., 2009. Tetraether membrane lipid distributions in water-column particulate matter and sediments: A study of 47 European lakes along a north-south transect. Journal of Paleolimnology 41, 523–540. https://doi.org/10.1007/s10933-008-9242-2.

Blome, M.W., Cohen, A.S., Tryon, C.A., Brooks, A.S., Russell, J., 2012. The environmental context for the origins of modern human diversity: A synthesis of regional variability in African climate 150,000–30,000 years ago. Journal of Human Evolution 62, 563-592. https://doi.org/10.1016/j.jhevol.2012.01.011.

Bodé, S., De Wispelaere, L., Hemp, A., Verschuren, D., Boeckx, P., 2020. Water-isotope ecohydrology of Mount Kilimanjaro. Ecohydrology 13, e2171. https://doi.org/10.1002/eco.2171.

Brassell, S.C., Eglinton, G., Marlowe, I.T., Pflaumann, U., Sarnthein, M., 1986. Molecular stratigraphy: A new tool for climatic assessment. Nature 320, 129–133. https://doi.org/10.1038/320129a0.

Buckles, L.K., Weijers, J.W.H., Verschuren, D., Sinninghe Damsté, J.S., 2014. Sources of core and intact branched tetraether membrane lipids in the lacustrine environment: Anatomy of Lake Challa and its catchment, equatorial East Africa. Geochimica et Cosmochimica Acta 140, 106–126. https://doi.org/10.1016/j.gca.2014.04.042.

Castañeda, I.S., Schouten, S., 2011. A review of molecular organic proxies for examining modern and ancient lacustrine environments. Quaternary Science Reviews 30, 2851–2891. https://doi.org/10.1016/j.quascirev.2011.07.009.

Chen, Y., Zheng, F., Yang, H., Yang, W., Wu, R., Liu, X., Liang, H., Chen, H., Pei, H., Zhang, C., Pancost, R.D., Zeng, Z., 2022. The production of diverse brGDGTs by an Acidobacterium providing a physiological basis for paleoclimate proxies. Geochimica et Cosmochimica Acta 337, 155–165.

Cramwinckel, M.J., van der Ploeg, R., van Helmond, N.A., Waarlo, N., Agnini, C., Bijl, P. K., van der Boon, A., Brinkhuis, H., Frieling, J., Krijgsman, W., Mather, T.A., Middelburg, J.J., Peterse, F., Slomp, C.P., Sluijs, A., 2022. Deoxygenation and organic carbon sequestration in the Tethyan realm associated with the middle Eocene climatic optimum. GSA Bulletin 135, 1280–1296. https://doi.org/10.1130/b36280.1.

De Crop, W., Verschuren, D., 2019. Determining patterns of stratification and mixing in tropical crater lakes through intermittent water-column profiling: A case study in western Uganda. Journal of African Earth Sciences 153, 17–30. https://doi.org/10.1016/j.jafrearsci.2019.02.019.

De Jonge, C., Hopmans, E.C., Stadnitskaia, A., Rijpstra, W.I.C., Hofland, R., Tegelaar, E., Sinninghe Damsté, J.S., 2013. Identification of novel penta- and hexamethylated branched glycerol dialkyl glycerol tetraethers in peat using HPLC-MS2, GC-MS and GC-SMB-MS. Organic Geochemistry 54, 78–82. https://doi.org/10.1016/j.orggeochem.2012.10.004.

De Jonge, C., Hopmans, E.C., Zell, C.I., Kim, J.H., Schouten, S., Sinninghe Damsté, J.S., 2014. Occurrence and abundance of 6-methyl branched glycerol dialkyl glycerol tetraethers in soils: Implications for palaeoclimate reconstruction. Geochimica et Cosmochimica Acta 141, 97–112. https://doi.org/10.1016/j.gca.2014.06.013.

De Jonge, C., Radujkovic, D., Sigurdsson, B.D., Weedon, J.T., Janssens, I., Peterse, F., 2019. Lipid biomarker temperature proxy responds to abrupt shift in the bacterial community composition in geothermally heated soils. Organic Geochemistry 137, 103897. https://doi.org/10.1016/j.orggeochem.2019.07.006.

De Wispelaere, L., Bodé, S., Hervé-Fernández, P., Hemp, A., Verschuren, D., Boeckx, P., 2017. Plant water resource partitioning and isotopic fractionation during transpiration in a seasonally dry tropical climate. Biogeosciences 14, 73–88. https://doi.org/10.5194/bg-14-73-2017.

Elling, F.J., Kattein, L., Naafs, B.D.A., Lauretano, V., Pearson, A., 2023. Heterotrophic origin and diverse sources of branched glycerol monoalkyl glycerol tetraethers (brGMGTs) in peats and lignites. Organic Geochemistry 178, 104558. https://doi.org/10.1016/j.orggeochem.2023.104558.

Frieling, J., Bohaty, S.M., Cramwinckel, M.J., Gallagher, S.J., Holdgate, G.R., Reichgelt, T., Peterse, F., Pross, J., Sluijs, A., Bijl, P.K., 2023. Revisiting the Geographical Extent of Exceptional Warmth in the Early Paleogene Southern Ocean. Paleoceanography and Paleoclimatology 38, e2022PA004529. https://doi.org/10.1029/2022pa004529.

Garcia, A.A., Chadwick, G.L., Welander, P.V., 2023. Discovery of two archaeal GDGT lipid modifying enzymes reveals diverse microbes capable of H-GDGT biosynthesis and modification. bioRxiv 2023 – 10. https://doi.org/10.1101/2023.10.20.563219.

Griepentrog, M., De Wispelaere, L., Bauters, M., Bodé, S., Hemp, A., Verschuren, D., Boeckx, P., 2019. Influence of plant growth form, habitat and season on leaf-wax n-alkane hydrogen-isotopic signatures in equatorial East Africa. Geochimica et Cosmochimica Acta 263, 122–139. https://doi.org/10.1016/j.gca.2019.08.004.

Halamka, T.A., Raberg, J.H., McFarlin, J.M., Younkin, A.D., Mulligan, C., Liu, X.L., Kopf, S.H., 2023. Production of diverse brGDGTs by Acidobacterium Solibacter usitatus in response to temperature, pH, and O2 provides a culturing perspective on brGDGT proxies and biosynthesis. Geobiology 21, 102–118. https://doi.org/10.1111/gbi.12525.

Hemp, A., 2006. Continuum or zonation? Altitudinal gradients in the forest vegetation of Mt. Kilimanjaro. Plant Ecology 184, 27–42. https://doi.org/10.1007/s11258-005-9049-4.

Hopmans, E.C., Schouten, S., Sinninghe Damsté, J.S., 2016. The effect of improved chromatography on GDGT-based palaeoproxies. Organic Geochemistry 93, 1–6. https://doi.org/10.1016/j.orggeochem.2015.12.006.

Huguet, C., de Lange, G.J., Gustafsson, Ö., Middelburg, J.J., Sinninghe Damsté, J.S., Schouten, S., 2008. Selective preservation of soil organic matter in oxidized marine sediments (Madeira Abyssal Plain). Geochimica et Cosmochimica Acta 72, 6061–6068.

Huguet, C., Schimmelmann, A., Thunell, R., Lourens, L.J., Sinninghe Damsté, J.S., Schouten, S., 2007. A study of the TEX_{86} paleothermometer in the water column and sediments of the Santa Barbara Basin, California. Paleoceanography 22, PA3203. https://doi.org/10.1029/2006PA001310.

Inglis, G.N., Bhattacharya, T., Hemingway, J.D., Hollingsworth, E.H., Feakins, S.J., Tierney, J.E., 2022. Biomarker Approaches for Reconstructing Terrestrial Environmental Change. Annual Review of Earth and Planetary Sciences 50, 354–369. https://doi.org/10.1146/annurev-earth-032320-095943.

Jaeschke, A., Jørgensen, S.L., Bernasconi, S.M., Pedersen, R.B., Thorseth, I.H., Früh-Green, G.L., 2012. Microbial diversity of Loki's Castle black smokers at the Arctic Mid-Ocean Ridge. Geobiology 10, 548–561. https://doi.org/10.1111/gbi.12009.

Jia, C., Zhang, C.L., Xie, W., Wang, J.X., Li, F., Wang, S., Dong, H., Li, W., Boyd, E.S., 2014. Differential temperature and pH controls on the abundance and composition of H-GDGTs in terrestrial hot springs. Organic Geochemistry 75, 109–121. https://doi.org/10.1016/j.orggeochem.2014.06.009.

Kim, J.H., van der Meer, J., Schouten, S., Helmke, P., Willmott, V., Sangiorgi, F., Koç, N., Hopmans, E.C., Sinninghe Damsté, J.S., 2010. New indices and calibrations derived from the distribution of crenarchaeal isoprenoid tetraether lipids: Implications for past sea surface temperature reconstructions. Geochimica et Cosmochimica Acta 74, 4639–4654. https://doi.org/10.1016/j.gca.2010.05.027.

Kirkels, F.M., Usman, M.O., Peterse, F., 2022. Distinct sources of bacterial branched GMGTs in the Godavari River basin (India) and Bay of Bengal sediments. Organic Geochemistry 167, 104405. https://doi.org/10.1016/j.orggeochem.2022.104405.

Knappy, C.S., Nunn, C.E., Morgan, H.W., Keely, B.J., 2011. The major lipid cores of the archaeon Ignisphaera aggregans: Implications for the phylogeny and biosynthesis of glycerol monoalkyl glycerol tetraether isoprenoid lipids. Extremophiles 15, 517–528. https://doi.org/10.1007/s00792-011-0382-3.

Lewis, W.M., 1987. Tropical limnology. Annual review of ecology and systematics 18, 159–184. https://doi.org/10.1146/annurev.es.18.110187.001111.

Li, Y., Yu, T., Feng, X., Zhao, B., Chen, H., Connock, G.T., Liu, X.L., Yang, H., Kaiser, J., Wittenborn, A.K., et al., 2023. Biosynthesis of H-GDGTs linked to ocean oxygen deficiency. BioRxiv, 2023–10. https://doi.org/10.1101/2023.10.20.562873.

Lisiecki, L.E., Raymo, M.E., 2005. A Pliocene-Pleistocene stack of 57 globally distributed benthic $\delta^{18}O$ records. Paleoceanography 20, PA1003. https://doi.org/10.1029/2004PA001071.

Liu, X.L., Summons, R.E., Hinrichs, K.U., 2012. Extending the known range of glycerol ether lipids in the environment: Structural assignments based on tandem mass spectral fragmentation patterns. Rapid Communications in Mass Spectrometry 26, 2295–2302. https://doi.org/10.1002/rcm.6355.

Loomis, S.E., Russell, J.M., Verschuren, D., Morrill, C., Cort, G.D., Sinninghe Damsté, J. S., Olago, D., Eggermont, H., Street-Perrott, F.A., Kelly, M.A., 2017. The tropical lapse rate steepened during the Last Glacial Maximum. Science Advances 3, e1600815. https://doi.org/10.1126/sciadv.1600815.

Lutnaes, B.F., Brandal, Øystein, Sjöblom, J., Krane, J., 2006. Archaeal C_{80} isoprenoid tetraacids responsible for naphthenate deposition in crude oil processing. Organic and Biomolecular Chemistry 4, 616–620. https://doi.org/10.1039/b516907k.

Lutnaes, B.F., Krane, J., Smith, B.E., Rowland, S.J., 2007. Structure elucidation of C_{80}, C_{81} and C_{82} isoprenoid tetraacids responsible for naphthenate deposition in crude oil production. Organic and Biomolecular Chemistry 5, 1873–1877. https://doi.org/10.1039/b701462g.

Lê, S., Josse, J., Husson, F., 2008. FactoMineR: An R package for multivariate analysis. Journal of Statistical Software 25, 1–18. https://doi.org/10.18637/jss.v025.i01.

Maitituerdi, A., Daele, M.V., Verschuren, D., Batist, M.D., Waldmann, N., 2022. Depositional history of Lake Chala (Mt. Kilimanjaro, equatorial East Africa) from high-resolution seismic stratigraphy. Journal of African Earth Sciences 189, 104499. https://doi.org/10.1016/j.jafrearsci.2022.104499.

Martin-Jones, C., Lane, C., Daele, M.V., Van Der Meeren, T., Wolff, C., Moorhouse, H., Tomlinson, E., Verschuren, D., 2020. History of scoria-cone eruptions on the eastern shoulder of the Kenya-Tanzania Rift revealed in the 250-ka sediment record of Lake Chala near Mount Kilimanjaro. Journal of Quaternary Science 35, 245–255. https://doi.org/10.1002/jqs.3140.

Moernaut, J., Verschuren, D., Charlet, F., Kristen, I., Fagot, M., Batist, M.D., 2010. The seismic-stratigraphic record of lake-level fluctuations in Lake Challa: Hydrological stability and change in equatorial East Africa over the last 140 kyr. Earth and Planetary Science Letters 290, 214–223. https://doi.org/10.1016/j.epsl.2009.12.023.

Morii, H., Eguchi, T., Nishihara, M., Kakinuma, K., König, H., Koga, Y., 1998. A novel ether core lipid with H-shaped C80-isoprenoid hydrocarbon chain from the hyperthermophilic methanogen Methanothermus fervidus. Biochimica et Biophysica Acta - Lipids and Lipid Metabolism 1390, 339–345. https://doi.org/10.1016/S0005-2760(97)00183-5.

Naafs, B.D.A., Inglis, G.N., Zheng, Y., Amesbury, M.J., Biester, H., Bindler, R., Blewett, J., Burrows, M.A., del Castillo Torres, D., Chambers, F.M., Cohen, A.D., Evershed, R.P., Feakins, S.J., Gałka, M., Gallego-Sala, A., Gandois, L., Gray, D.M., Hatcher, P.G., Honorio Coronado, E.N., Hughes, P.D.M., Huguet, A., Könönen, M., Laggoun-Défarge, F., Lähteenoja, O., Lamentowicz, M., Marchant, R., McClymont, E., Pontevedra-Pombal, X., Ponton, C., Pourmand, A., Rizzuti, A.M., Rochefort, L., Schellekens, J., De Vleeschouwer, F., Pancost, R.D., 2017. Introducing global peat-specific temperature and pH calibrations based on brGDGT bacterial lipids. Geochimica et Cosmochimica Acta 208, 285–301. https://doi.org/10.1016/j.gca.2017.01.038.

Naafs, B.D., McCormick, D., Inglis, G.N., Pancost, R.D., 2018. Archaeal and bacterial H-GDGTs are abundant in peat and their relative abundance is positively correlated with temperature. Geochimica et Cosmochimica Acta 227, 156–170. https://doi.org/10.1016/j.gca.2018.02.025.

Otto-Bliesner, B.L., Brady, E.C., Clauzet, G., Tomas, R., Levis, S., Kothavala, Z., 2006. Last glacial maximum and Holocene climate in CCSM3. Journal of Climate 19, 2526–2544. https://doi.org/10.1175/JCLI3748.1.

Pan, A., Yang, Q., Zhou, H., Ji, F., Wang, H., Pancost, R.D., 2016. A diagnostic GDGT signature for the impact of hydrothermal activity on surface deposits at the Southwest Indian Ridge. Organic Geochemistry 99, 90–101. https://doi.org/10.1016/j.orggeochem.2016.07.001.

Payne, B.R., 1970. Water balance of Lake Chala and its relation to groundwater from tritium and stable isotope data. Journal of Hydrology 11, 47–58. https://doi.org/10.1016/0022-1694(70)90114-9.

Pearson, E.J., Juggins, S., Talbot, H.M., Weckström, J., Rosén, P., Ryves, D.B., Roberts, S. J., Schmidt, R., 2011. A lacustrine GDGT-temperature calibration from the Scandinavian Arctic to Antarctic: Renewed potential for the application of GDGT-paleothermometry in lakes. Geochimica et Cosmochimica Acta 75, 6225–6238. https://doi.org/10.1016/j.gca.2011.07.042.

Powers, L., Werne, J.P., Vanderwoude, A.J., Sinninghe Damsté, J.S., Hopmans, E.C., Schouten, S., 2010. Applicability and calibration of the TEX_{86} paleothermometer in lakes. Organic Geochemistry 404–413. https://doi.org/10.1016/j.orggeochem.2009.11.009.

Powers, L.A., Werne, J.P., Johnson, T.C., Hopmans, E.C., Sinninghe Damsté, J.S., Schouten, S., 2004. Crenarchaeotal membrane lipids in lake sediments: A new paleotemperature proxy continental paleoclimate reconstruction? Geology 32, 613–616. https://doi.org/10.1130/G20434.1.

Prahl, F.G., Wakeham, S.G., 1987. Calibration of unsaturation patterns in long-chain ketone compositions for palaeotemperature assessment. Nature 330, 367–369. https://doi.org/10.1038/330367a0.

Raberg, J.H., Miller, G.H., Geirsdóttir, Áslaug, Sepúlveda, J., 2022. Near-universal trends in brGDGT lipid distributions in nature. Science Advances 8, eabm7625. https://doi.org/10.1126/sciadv.abm7625.

Sahonero-Canavesi, D.X., Siliakus, M.F., Abdala Asbun, A., Koenen, M., von Meijenfeldt, F.B., Boeren, S., Bale, N.J., Engelman, J.C., Fiege, K., Strack van Schijndel, L., et al., 2022. Disentangling the lipid divide: Identification of key enzymes for the biosynthesis of membrane-spanning and ether lipids in Bacteria. Science Advances 8, eabq8652. https://doi.org/10.1126/sciadv.abq8652.

Schouten, S., Baas, M., Hopmans, E.C., Sinninghe Damsté, J.S., 2008. An unusual isoprenoid tetraether lipid in marine and lacustrine sediments. Organic Geochemistry 39, 1033–1038. https://doi.org/10.1016/j.orggeochem.2008.01.019.

Schouten, S., Baas, M., Hopmans, E.C., Reysenbach, A.L., Sinninghe Damsté, J.S., 2008. Tetraether membrane lipids of Candidatus "Aciduliprofundum boonei", a cultivated obligate thermoacidophilic euryarchaeote from deep-sea hydrothermal vents. Extremophiles 12, 119–124.

Schouten, S., Hopmans, E.C., Sinninghe Damsté, J.S., 2013. The organic geochemistry of glycerol dialkyl glycerol tetraether lipids: A review. Organic Geochemistry 54, 19–61. https://doi.org/10.1016/j.orggeochem.2012.09.006.

Schouten, S., Hopmans, E.C., Schefuß, E., Sinninghe Damste, J.S., 2002. Distributional variations in marine crenarchaeotal membrane lipids: a new tool for reconstructing ancient sea water temperatures? Earth and Planetary Science Letters 204, 265–274.

Sinninghe Damsté, J.S., Hopmans, E.C., Pancost, R.D., Schouten, S., Geenevasen, J.A., 2000. Newly discovered non-isoprenoid glycerol dialkyl glycerol tetraether lipids in sediments. Chemical 2000, 1683–1684. https://doi.org/10.1039/b004517i.

Sinninghe Damsté, J.S., Ossebaar, J., Abbas, B., Schouten, S., Verschuren, D., 2009. Fluxes and distribution of tetraether lipids in an equatorial African lake: Constraints on the application of the TEX_{86} palaeothermometer and BIT index in lacustrine settings. Geochimica et Cosmochimica Acta 73, 4232–4249. https://doi.org/10.1016/j.gca.2009.04.022.

Sinninghe Damsté, J.S., Ossebaar, J., Schouten, S., Verschuren, D., 2008. Altitudinal shifts in the branched tetraether lipid distribution in soil from Mt. Kilimanjaro (Tanzania): Implications for the MBT/CBT continental palaeothermometer. Organic Geochemistry 39, 1072–1076. https://doi.org/10.1016/j.orggeochem.2007.11.011.

Sinninghe Damsté, J.S., Rijpstra, W.I.C., Foesel, B.U., Huber, K.J., Overmann, J., Nakagawa, S., Kim, J.J., Dunfield, P.F., Dedysh, S.N., Villanueva, L., 2018. An overview of the occurrence of ether- and ester-linked iso-diabolic acid membrane lipids in microbial cultures of the Acidobacteria: Implications for brGDGT paleoproxies for temperature and pH. Organic Geochemistry 124, 63–76. https://doi.org/10.1016/j.orggeochem.2018.07.006.

Sinninghe Damsté, J.S., Rijpstra, W.I.C., Hopmans, E.C., Foesel, B.U., Wüst, P.K., Overmann, J., Tank, M., Bryant, D.A., Dunfield, P.F., Houghton, K., Stott, M.B., 2014. Ether- and ester-bound iso-diabolic acid and other lipids in members of Acidobacteria subdivision 4. Applied and Environmental Microbiology 80. https://doi.org/10.1128/AEM.01066-14.

Sinninghe Damsté, J.S., Rijpstra, W.I.C., Hopmans, E.C., Weijers, J.W., Foesel, B.U., Overmann, J., Dedysh, S.N., 2011. 13,16-Dimethyl octacosanedioic acid (iso-Diabolic Acid), a common membrane-spanning lipid of Acidobacteria subdivisions 1 and 3. Applied and Environmental Microbiology 77. https://doi.org/10.1128/AEM.00466-11.

Sluijs, A., Frieling, J., Inglis, G.N., Nierop, K.G., Peterse, F., Sangiorgi, F., Schouten, S., 2020. Late Paleocene-early Eocene Arctic Ocean sea surface temperatures: Reassessing biomarker paleothermometry at Lomonosov Ridge. Climate of the Past 16, 2381–2400. https://doi.org/10.5194/cp-16-2381-2020.

Swai, V., 2018. Lake Chala statigraphy: Developing a method to identify and quantify surficial slope sediment remobilization. Ghent University, Belgium. Unpublished Masters thesis.

Tang, X., Naafs, B.D.A., Pancost, R.D., Liu, Z., Fan, T., Zheng, Y., 2021. Exploring the Influences of Temperature on "H-Shaped" Glycerol Dialkyl Glycerol Tetraethers in a Stratigraphic Context: Evidence From Two Peat Cores Across the Late Quaternary. Frontiers in Earth Science 8, 541685 doi:10.3389/feart.2020.541685.

Tierney, J.E., Russell, J.M., Eggermont, H., Hopmans, E.C., Verschuren, D., Sinninghe Damsté, J.S., 2010. Environmental controls on branched tetraether lipid distributions in tropical East African lake sediments. Geochimica et Cosmochimica Acta 74, 4902–4918. https://doi.org/10.1016/j.gca.2010.06.002.

van Geel, B., Kristen, I., Plessen, B., Lyaruu, A., Engstrom, D.R., van der Plicht, J., Verschuren, D., Blaauw, M., 2011. High-resolution C-14 dating of a 25,000-year lake-sediment record from equatorial East Africa. Quaternary Science Reviews 30, 3043–3059. https://doi.org/10.1016/j.quascirev.2011.07.014.

van Bree, L.G., Peterse, F., Baxter, A.J., De Crop, W., Van Grinsven, S., Villanueva, L., Verschuren, D., Sinninghe Damsté, J.S., 2020. Seasonal variability and sources of in situ brGDGT production in a permanently stratified African crater lake. Biogeosciences 17, 5443–5463. https://doi.org/10.5194/bg-17-5443-2020.

van Bree, L.G., Peterse, F., van der Meer, M.T., Middelburg, J.J., Negash, A.M., Crop, W. D., Cocquyt, C., Wieringa, J.J., Verschuren, D., Sinninghe Damsté, J.S., 2018. Seasonal variability in the abundance and stable carbon-isotopic composition of lipid biomarkers in suspended particulate matter from a stratified equatorial lake (Lake Chala, Kenya/Tanzania): Implications for the sedimentary record. Quaternary Science Reviews 192, 208–224. https://doi.org/10.1016/j.quascirev.2018.05.023.

Verschuren, D., Sinninghe Damsté, J.S., Moernaut, J., Kristen, I., Blaauw, M., Fagot, M., Haug, G.H., 2009. Half-precessional dynamics of monsoon rainfall near the East African Equator. Nature 462, 637–641. https://doi.org/10.1038/nature08520.

Verschuren, D., Olagod, D.O., Rucina, S.M., Odhengo, P.O., 2013. DeepCHALLA: Two glacial cycles of climate and ecosystem dynamics from equatorial East Africa. Scientific 52, 72–76. https://doi.org/10.2204/iodp.sd.15.09.2013.

Wainwright, C.M., Marsham, J.H., Keane, R.J., Rowell, D.P., Finney, D.L., Black, E., Allan, R.P., 2019. 'Eastern African Paradox' rainfall decline due to shorter not less intense Long Rains. npj Climate and Atmospheric Science 2, 34. https://doi.org/10.1038/s41612-019-0091-7.

Weber, Y., Damsté, J.S.S., Zopfi, J., De Jonge, C., Gilli, A., Schubert, C.J., Lepori, F., Lehmann, M.F., Niemann, H., 2018. Redox-dependent niche differentiation of tetraether producing bacteria: Evidence for multiple branched GDGT sources in lakes. Proceedings of the National Academy of Sciences of the United States of America 115, 10926–10931. https://doi.org/10.1073/pnas.1805186115.

Weijers, J.W., Panoto, E., van Bleijswijk, J., Schouten, S., Rijpstra, W.I.C., Balk, M., Stams, A.J., Sinninghe Damsté, J.S., 2009. Constraints on the biological source(s) of the orphan branched tetraether membrane lipids. Geomicrobiology Journal 26, 402–414. https://doi.org/10.1080/01490450902937293.

Weijers, J.W., Schouten, S., van den Donker, J.C., Hopmans, E.C., Sinninghe Damsté, J. S., 2007. Environmental controls on bacterial tetraether membrane lipid distribution in soils. Geochimica et Cosmochimica Acta 71, 703–713. https://doi.org/10.1016/j.gca.2006.10.003.

Weijers, J.W., Schouten, S., Hopmans, E.C., Geenevasen, J.A., David, O.R., Coleman, J. M., Pancost, R.D., Sinninghe Damsté, J.S., 2006. Membrane lipids of mesophilic anaerobic bacteria thriving in peats have typical archaeal traits. Environmental Microbiology 8, 648–657. https://doi.org/10.1111/j.1462-2920.2005.00941.x.

Weijers, J.W., Schouten, S., Spaargaren, O.C., Sinninghe Damsté, J.S., 2006. Occurrence and distribution of tetraether membrane lipids in soils: Implications for the use of the TEX_{86} proxy and the BIT index. Organic Geochemistry 37. https://doi.org/10.1016/j.orggeochem.2006.07.018.

Wolff, C., Haug, G.H., Timmermann, A., Sinninghe Damsté, J.S., Brauer, A., Sigman, D. M., Cane, M.A., Verschuren, D., 2011. Reduced interannual rainfall variability in East Africa during the last ice age. Science 333, 743–747. https://doi.org/10.1126/science.1203724.

Wolff, C., Kristen-Jenny, I., Schettler, G., Plessen, B., Meyer, H., Dulski, P., Naumann, R., Brauer, A., Verschuren, D., Haug, G.H., 2014. Modern seasonality in Lake Challa (Kenya/Tanzania) and its sedimentary documentation in recent lake sediments. Limnology and Oceanography 59, 1621–1636. https://doi.org/10.4319/lo.2014.59.5.1621.

Xie, S., Liu, X.L., Schubotz, F., Wakeham, S.G., Hinrichs, K.U., 2014. Distribution of glycerol ether lipids in the oxygen minimum zone of the Eastern Tropical North Pacific Ocean. Organic Geochemistry 71, 60–71. https://doi.org/10.1016/j.orggeochem.2014.04.006.

Zink, K.G., Leythaeuser, D., Melkonian, M., Schwark, L., 2001. Temperature dependency of long-chain alkenone distributions in Recent to fossil limnic sediments and in lake waters. Geochimica et Cosmochimica Acta 65, 253–265. https://doi.org/10.1016/S0016-7037(00)00509-3.